

Mathematical Analysis and Modeling of Ebola Virus Dynamics via Optimal Control and Neural Network Paradigms *

Noor Muhammad^{1,*}, Md. Nur Alam^{2,3}, Zhang Shiqing^{1,*}, and Ali Akgül⁴

¹School of Mathematics, Sichuan University, Chengdu, China, 610064

²School of Mathematical Sciences, Sunway University, Bandar Sunway, Petaling Jaya 47500, Selangor Darul Ehsan, Malaysia

³Department of Mathematics, Pabna University of Science & Technology, Pabna-6600, Bangladesh

⁴Siirt University, Art and Science Faculty, Department of Mathematics, 56100 Siirt, Turkey

*Corresponding authors: , ¹noormuhammad@stu.scu.edu.cn, noormustaffa681@gmail.com , ¹zhangshiqing@scu.edu.cn

Abstract

Ebola virus disease is a severe, often fatal infectious disease transmitted through direct contact with infected bodily fluids and contaminated surfaces. This study addresses the serious need for integrated predictive and control frameworks by developing a unified approach that connects intelligent outbreak prediction systems with mathematical models of Ebola transmission. We propose a novel nonlinear fractional-order eight-compartment SVEI_sI_aHDR model that integrates control measures, personal protection, vaccination, treatment, and safe burial to analyze their effectiveness in reducing Ebola transmission and improving outbreak prediction. Mathematical validation establishes the model's boundedness, non-negativity, and well-posedness. We derive the basic reproduction number R_0 via the next-generation matrix, identify disease-free and endemic equilibrium, and conduct stability analyses. Sensitivity analysis reveals R_0 's primary sensitivity to transmission rate β (+1.00), incubation period σ (+0.6250), and infectivity of the dead η_d (+0.4678). An optimal control framework minimizes disease management costs (4 dollars per infection). Numerical simulation by the RK45 method demonstrates combined treatment and safe burial controls 86.5% of target morbidity and mortality, with safe burial being the most effective single measure. We develop a disease-informed neural network (DINN) achieving 99.87% prediction accuracy ($R^2 = 0.9987$) with minimal error (NMSE 10^{-4} to 10^{-5}). The DINN accurately recovers 13 of 17 transmission parameters with < 9% error, establishing a new interpretability benchmark. This integrated framework provides public health officials with a practical tool to test interventions and predict outbreaks through model-data integration.

Keywords: Ebola virus disease, fractional-order compartmental model, basic reproduction number (R_0), optimal control, sensitivity analysis, stability analysis, outbreak prediction, disease-informed neural network (DINN).

1 Introduction

A serious infectious disease, Ebola Virus Disease (EVD) is transmitted to people by reservoirs of animals such as fruit bats. When the Ebola virus transmits from animal reservoirs into human populations, an outbreak occurs [1, 2]. The illness has historically significant case fatality rates, with outbreaks ranging from 25% to 90% [3]. It was first reported in the Democratic Republic of the Congo in 1976; the name Ebola was given due to the Ebola River [4]. With 28,646 confirmed infections and 11,323 deaths recorded, the most catastrophic epidemic was in West Africa (2014–2016), with almost a 50% death ratio [5]. Fever, weakness, diarrhea, and, in extreme situations, hemorrhagic signs are common in infected people. There is a major issue in that these viruses' incubation periods differ, sometimes 2 days and sometimes 21 days; infected individuals cannot

*A preliminary version of this work is available on arXiv: <https://arxiv.org/abs/2511.06303> or via DOI: <https://doi.org/10.48550/arXiv.2511.06303>.

spread the virus throughout the incubation phase [6]. Fruit bats are considered to be the main natural source of infection in humans, and non-human primates serve as end hosts, maintaining cycles of transmission that can result in major outbreaks [7, 8]. Controlling measures are complicated, particularly frequent contact paths that boost the spread of EVD. Being in contact with infectious body fluids, such as blood or excretions, results in subsequent human-to-human transmission. Contact with deceased individuals during traditional burial practices is a crucial and widely recognized route of transmission that has been a significant facilitator of prior epidemics [9, 10]. In addition, the virus might continue to spread indirectly by remaining on contaminated surfaces. Due to the absence of apparent symptoms, various demographic categories, in particular people who participate in burial customs and asymptomatic individuals, have a possibility to spread infection throughout communities. Therefore, it is difficult for standard mathematical models to capture the EVD dynamics of transmission, as they have to immediately identify these various and context-specific threats [11, 12]. Ebola transmission is rendered much more difficult by the potential for reinfection. After recovery, immunity may not be total or long-lasting because protective antibodies may gradually decline in survivors [13, 14]. Individuals who have previously been infected can test positive for the virus years later, indicating potential re-exposure and infection, according to data from previous outbreaks [15, 16]. Additionally, research on populations that have been exposed frequently has discovered people who display no symptoms but do not have detectable antibodies, underscoring the heterogeneity in immune response [17, 18]. Now, we focus on a few equivalent mathematical models of EVD that have already been proposed by other researchers. Fractional calculus has been applied to infectious disease modeling in a number of research investigations, displaying more consistency with observed outbreak data than traditional approaches [19, 20]. Fractional calculus has long shown the potential to model memory effects and other non-local connections and thus provides a well-intentioned framework of study to overcome some of the noted deficiencies [21]. Unlike integer-order derivatives, which always adopt Markovian processes, fractional operators capture the distributed suspensions that are characteristic of epidemiological systems, such as extended incubation periods, waning immunity, and environmental reservoirs of pathogens [22]. Evidence of progress in the modeling of infectious diseases for which data are available and for which fractional calculus applies exhibits greater concord with experimental indication, especially for diseases with long-range chronological correlations and power law decline in the efficiency of involvements [23, 24]. The non-Markovian nature of some fractional derivatives offers a better-suited mathematical framework for modeling the transmission of disease in and among structured populations [25]. The SI model, such as [26, 27], the SEIR model [28, 29], the SEIRD model [30], and the SEIRHD model [31, 32, 33, 34], where S , E , I , H , R , and D represent susceptible, exposed, infectious, hospitalized, recovered, and dead/deceased compartments, respectively [35], separated the Dead/Deceased (D) compartment into two compartments, buried deceased (R_D) and unburied dead (F). Similarly, in their SIRPD model, where P represents environmental contamination, [26] included EVD transmission through contaminated surroundings of deceased patients. While models like the SEIHFDBR in [36] represent notable developments, they remain limited by their integer-order formulation. Understanding how to effectively control the spread of infection and facilitate decision-making during an epidemic is one of the applications of mathematical modeling. For example, [37] presented an SIR model-based optimum control issue with treatment and immunization as possible control strategies. They looked into the most effective vaccination and therapy combinations to lower the cost of those preventive measures. In [38] investigated various diseases transmitted by insects that directly infect the host population, such as dengue fever, malaria, and the West Nile virus, using optimal control analysis. In order to examine the transmission of Ebola, [39] designed a model. They evaluated the effects of various preventative measures such as vaccination, public awareness campaigns, early identification campaigns, improved hospital sanitation, separation of people with infections, and geographical constraints. Another field of research is the integration of machine learning with traditional epidemiological models. When handling noisy or incomplete surveillance information, physics-informed neural networks (PINNs) demonstrate particular potential for parameter estimation and prediction [40, 41, 42]. A comprehensive analysis of the last five years' worth of literature, however, reveals enduring shortcomings and disparate study directions. Although fractional models have been created, they are frequently not integrated with intricate multi-pathway transmission designs specific to EVD, for instance. Likewise, machine learning applications often function independently of mathematical models, which limits their understanding and generalization, and optimal control formulations usually use simplified models that do not fully capture the complexity of transmission dynamics [43]. Nevertheless, despite these

developments, there are still important research gaps in present literature. Firstly, there is a gap between the full representation of all recognized EVD transmission channels (symptomatic, asymptomatic, and burial customs) and fractional-order models, which account for memory effects. There is a methodological gap given that detailed transmission models generally employ integer-order approaches, whereas the majority of fractional models simplify transmission dynamics. Second, the application of optimal control theory to high-dimensional fractional systems that reflect EVD dynamics has been insufficient. One major challenge that has limited practical applicability is the mathematical complexity of determining optimal control policies for such systems, especially when including numerous intervention strategies with different costs and effectiveness. [44, 45]. Third, the majority of applications currently only combine biological process-based models with data-driven machine learning techniques. Hybrid frameworks have been proposed, but they typically lack the seamless combination needed for real-time parameter estimation and prediction during current outbreaks [46]. This study develops a novel computational framework with the particular objectives that follow in order to address these connected challenges. The practical objective is to provide public health decision-makers an efficient computational tool that can forecast disease paths with measured uncertainty, optimize allocation of resources for maximum impact, and simulate outbreak scenarios under different intervention strategies. The following is a list of this study's primary innovations and contributions:

- We developed a novel nonlinear fractional-order eight-compartment mathematical model with memory effects and multiple control intervention evaluation of Ebola transmission dynamics. To prove the validity of the model, we presented boundedness, positivity, and well-posedness. We obtained the basic reproduction number R_0 by the next-generation matrix approach and the disease-free and endemic equilibrium points and then conducted thorough stability analysis of both states. Through sensitivity analysis, we determined that parameters such as the transmission rate, the incubation period, and the infectivity of the deceased had the greatest effects on R_0 .
- We established the optimal control model that would help to reduce the cost of managing the disease by considering four intervention measures that included personal protection, vaccination, treatment and safe burial. Our theoretical analysis by applying Pontryagin's Maximum Principle and numerical simulation using the RK45 method permitted identifying the cost-effective strategies, and the level of their effectiveness in terms of transmission and mortality reduction.
- Motivated from physics-informed neural networks, we designed a new framework for disease-informed neural networks (DINN). This computational approach achieves high prediction accuracy across all disease stages and demonstrates strong parameter recovery capability, providing an interpretable tool for outbreak forecasting and intervention assessment.

This work significantly improves both academic research and healthcare practice by successfully addressing the existing gap between theoretical modeling and actual application. It offers investigators a new methodological framework that shows how machine learning, optimal control theory, and fractional calculus may be successfully used for the scientific study of infectious diseases. This paper proceeds as follows. In Section 2, I discuss the elementary ideas of fractional calculus, which is key to developing the model. In Section 3, I develop an eight-compartment, fractional-order Ebola transmission model. Section 4 presents the complete mathematical analysis of the model, including proofs of existence and uniqueness of solutions, identification of the invariant region and attractivity, derivation of the basic reproduction number (\mathcal{R}_0), and both local and global stability analyses for the disease-free and endemic equilibrium points. Section 5 performs a global sensitivity analysis that attempts to quantify and prioritize the impact of key model parameters on the disease transmission dynamics. Section 6 establishes and solves optimal control problem through the Maximum Principle of Pontryagin founding the most effective intervention strategies. In section 7, the formation of a disease-informed neural network (DINN) model along with the relevant numerical data is developed and fully analyzed. Lastly, in Section 8 the main findings are synthesized, the methodological limitations are critically discussed, and future research directions outlined.

2 Preliminaries

This part sets out the basic principles of fractional calculus which is essential to the construction and analysis of our model.

Definition 2.1 *Let $\alpha \in (0, 1]$ and $u \in C^1([0, T])$. For any function u which is continuously differentiable*

in the closure $[0, T]$ the Caputo fractional derivative of order α is defined in [21] as follows.

$${}^C D_t^\alpha u(t) = \frac{1}{\Gamma(1-\alpha)} \int_0^t (t-\tau)^{-\alpha} u'(\tau) d\tau.$$

This operator is preferred for modeling dynamical systems as it accommodates standard initial conditions, and ${}^C D_t^\alpha u(t) \rightarrow u'(t)$ as $\alpha \rightarrow 1^-$, recovering the classical integer-order derivative.

Definition 2.2 The equilibrium point y^* of the fractional-order system ${}^C D_t^\alpha y(t) = f(t, y(t))$ is said to be Mittag-Leffler stable if

$$\|y(t) - y^*\| \leq [m(y(0) - y^*)E_{\alpha,1}(-\lambda t^\alpha)]^b.$$

where $\alpha \in (0, 1)$, $\lambda \geq 0$, $b > 0$, $m(0) = 0$, and $m(y) \geq 0$. Mittag-Leffler stability implies asymptotic stability [47].

Lemma 2.1 Let $\alpha \in (0, 1]$. An equilibrium point y^* of the autonomous system ${}^C D_t^\alpha y(t) = f(y(t))$ is asymptotically stable if all eigenvalues λ_i of the Jacobian matrix $J = \partial f / \partial y|_{y^*}$ satisfy the condition [47].

$$|\arg(\lambda_i)| > \frac{\alpha\pi}{2}, \quad \forall i.$$

This condition generalizes the classical Routh-Hurwitz criterion to fractional-order systems.

3 Model formulation

We formulate a Caputo fractional-order model ($\alpha \in (0, 1]$) that incorporates the multi-pathway transmission, memory effects, and time-varying interventions of Ebola. The governing system is given as follows.

$$\begin{aligned} {}^C D_t^\alpha S(t) &= \Lambda - \frac{c\beta S(I_s + \eta_a I_a + \eta_d D)}{N} + \omega V - (v + \mu)S, \\ {}^C D_t^\alpha V(t) &= vS - (1 - \varepsilon) \frac{c\beta V(I_s + \eta_a I_a + \eta_d D)}{N} - (\mu + \omega)V, \\ {}^C D_t^\alpha E(t) &= \frac{c\beta[S + (1 - \varepsilon)V](I_s + \eta_a I_a + \eta_d D)}{N} - (\mu + \sigma)E, \\ {}^C D_t^\alpha I_s(t) &= p\sigma E - (\gamma_s + \delta_s + h_s + \mu)I_s, \\ {}^C D_t^\alpha I_a(t) &= (1 - p)\sigma E - (\gamma_a + \mu)I_a, \\ {}^C D_t^\alpha H(t) &= h_s I_s - (\gamma_h + \delta_h + \mu)H, \\ {}^C D_t^\alpha D(t) &= \delta_s I_s + \delta_h H - \mu_d D, \\ {}^C D_t^\alpha R(t) &= \gamma_s I_s + \gamma_a I_a + \gamma_h H - \mu R. \end{aligned} \tag{1}$$

The force of infection is given by

$$\lambda = \frac{c\beta(I_s + \eta_a I_a + \eta_d D)}{N},$$

and for notational simplicity, we define the model as

$$\begin{aligned} q_0 &= (v + \mu), & q_1 &= (\mu + \omega), & q_2 &= (\mu + \sigma), \\ q_3 &= (\gamma_s + \delta_s + h_s + \mu), & q_4 &= (\gamma_a + \mu), & q_5 &= (\gamma_h + \delta_h + \mu), \\ q_6 &= \mu_d. \end{aligned}$$

The model parameters include natural mortality (μ) and recruitment (Λ), vaccination rate $v(t)$ with waning immunity (ω), and force of infection $\lambda(t)$ driving exposures. Exposed individuals (E) progress to infectious states at rate σ , splitting into symptomatic (I_s , proportion p) and asymptomatic (I_a , $1 - p$) pathways. Symptomatic cases face hospitalization (h_s), disease-induced mortality (δ_s), or recovery (γ_s). Asymptomatic and hospitalized individuals recover at rates γ_a and γ_h , respectively, with hospital mortality (δ_h). Deceased

individuals (D) transmit infection until safe burial (μ_d). Transmission coefficients β , η_a , and η_d govern infectivity from symptomatic, asymptomatic, and post-mortem sources. The system is governed by,

$$\begin{aligned}
{}^C D_t^\alpha S(t) &= \Lambda - \lambda S + \omega V - q_0 S, \\
{}^C D_t^\alpha V(t) &= \nu S - (1 - \varepsilon) \lambda V - q_1 V, \\
{}^C D_t^\alpha E(t) &= \lambda [S + (1 - \varepsilon) V] - q_2 E, \\
{}^C D_t^\alpha I_s(t) &= p \sigma E - q_3 I_s, \\
{}^C D_t^\alpha I_a(t) &= (1 - p) \sigma E - q_4 I_a, \\
{}^C D_t^\alpha H(t) &= h_s I_s - q_5 H, \\
{}^C D_t^\alpha D(t) &= \delta_s I_s + \delta_h H - \mu_d D, \\
{}^C D_t^\alpha R(t) &= \gamma_s I_s + \gamma_a I_a + \gamma_h H - \mu R.
\end{aligned} \tag{2}$$

The fractional-order system (2) is analyzed with the following initial conditions:

$$S(0) = S_0 \geq 0, \quad V(0) = V_0 \geq 0, \quad E(0) = E_0 \geq 0, \quad I_s(0) = I_{s0} \geq 0,$$

$$I_a(0) = I_{a0} \geq 0, \quad H(0) = H_0 \geq 0, \quad D(0) = D_0 \geq 0, \quad R(0) = R_0 \geq 0.$$

In this Caputo fractional formulation, the system in (2) captures the dynamics of Ebola transmission in an eight-dimensional frame. This construction involves ‘epidemic’ components such as susceptible (S), vaccinated (V), exposed (E), symptomatically (I_s) and asymptomatically (I_a) infectious, hospitalized (H), deceased (D), and recovery (R) stages, thus integrating the critical structure of underlying dynamics. Furthermore, the model participates in the fractional-order system of differential equations, thus inserting memory effects.

Table 1: Parameters for the fractional-order Ebola model.

Symbol	Description	Value	Range	Source
β	Transmission rate	0.287	0.2–0.4	[48]
η_d	Deceased infectiousness	0.734	0.5–0.9	[48]
η_a	Asymptomatic infectiousness	0.523	0.3–0.7	Assumed (Fitted)
σ	Incubation rate (day $^{-1}$)	0.094	0.05–0.15	[49]
p	Symptomatic proportion	0.712	0.5–0.8	[49]
γ_s	Symptomatic recovery (day $^{-1}$)	0.068	0.05–0.1	[26]
γ_a	Asymptomatic recovery (day $^{-1}$)	0.089	0.07–0.12	[26]
δ_s	Symptomatic death (day $^{-1}$)	0.103	0.05–0.15	[50]
δ_h	Hospitalized death (day $^{-1}$)	0.067	0.03–0.09	[50]
h_s	Hospitalization rate	0.312	0.2–0.4	[51]
Λ	Recruitment rate	100	100–1000	[52]
μ	Natural mortality (day $^{-1}$)	3.5×10^{-5}	–	[52]
$v(t)$	Vaccination rate	–	0.005–0.08	Assumed (Control)
ε	Vaccine efficacy	–	0.85–0.95	Assumed (Control)
ω	Waning immunity (day $^{-1}$)	–	0.0027–0.0037	Assumed
α	Fractional order	0.85	0.75–0.95	Assumed (Model)

4 Mathematical Analysis

4.1 Well-Posedness of the Model

We establish the mathematical well-posedness of the fractional-order Ebola system through existence and uniqueness analysis.

Theorem 4.1 *Given any $\alpha \in (0, 1]$, and initial conditions ae $\mathbf{X}_0 = (S_0, V_0, E_0, I_{s0}, I_{a0}, H_0, D_0, R_0) \in \mathbb{R}_+^8$, the fractional-order model (2) has the unique solution $\mathbf{X}(t) = (S(t), V(t), E(t), I_s(t), I_a(t), H(t), D(t), R(t))$ for all $t \geq 0$.*

Proof. Define the state vector $\mathbf{X}(t) = (S, V, E, I_s, I_a, H, D, R)^T$ and express the system as

$${}^C D_t^\alpha \mathbf{X}(t) = \mathbf{F}(t, \mathbf{X}(t)), \quad \mathbf{X}(0) = \mathbf{X}_0.$$

The equivalent Volterra integral formulation is

$$\mathbf{X}(t) = \mathbf{X}_0 + \frac{1}{\Gamma(\alpha)} \int_0^t (t-s)^{\alpha-1} \mathbf{F}(s, \mathbf{X}(s)) ds, \tag{3}$$

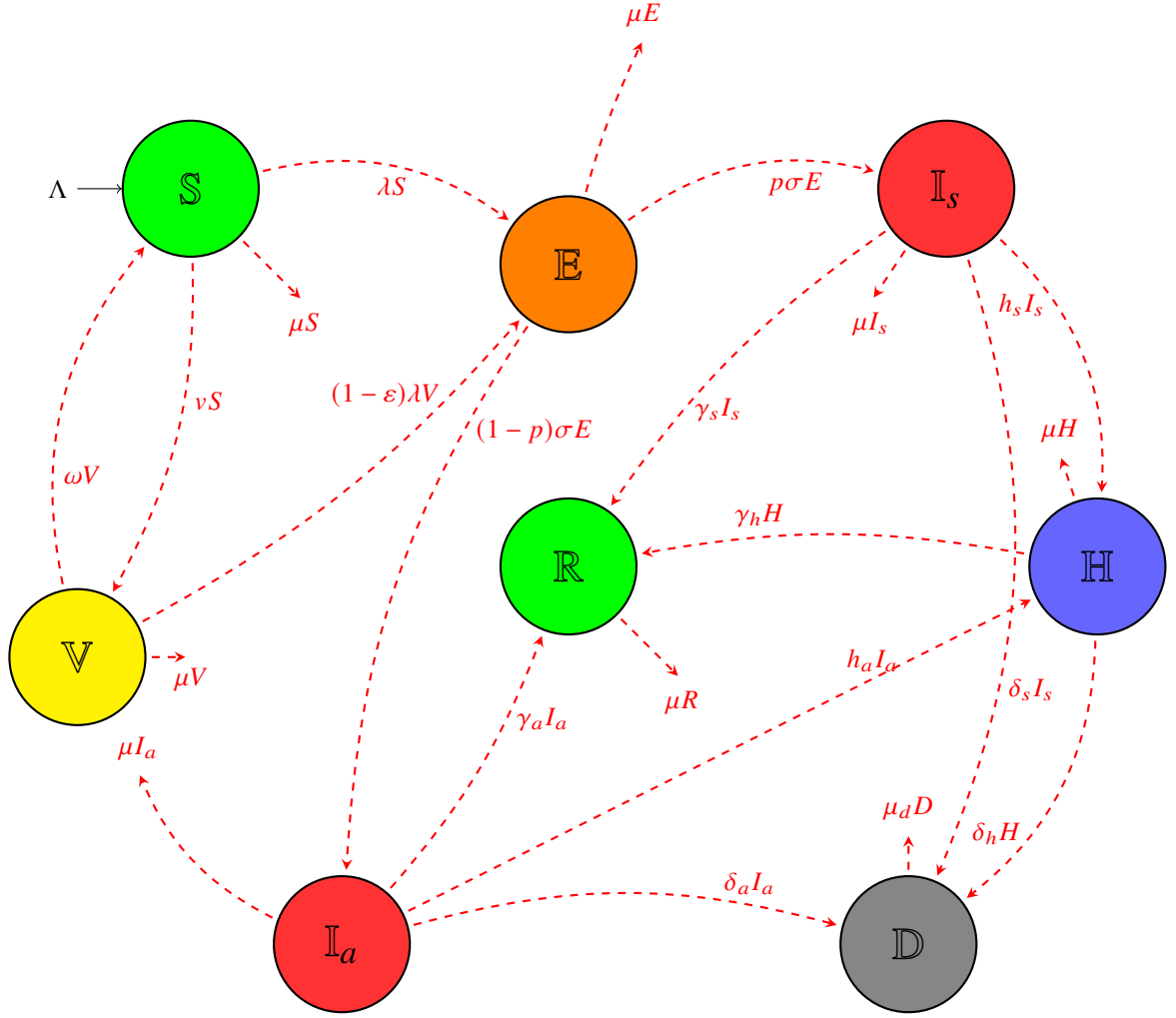


Figure 1: Transmission architecture of the fractional Ebola model.

Assume the operator $\mathcal{T} : C([0, T], \mathbb{R}^8) \rightarrow C([0, T], \mathbb{R}^8)$ defined by

$$(\mathcal{T}\mathbf{X})(t) = \mathbf{X}_0 + \frac{1}{\Gamma(\alpha)} \int_0^t (t-s)^{\alpha-1} \mathbf{F}(s, \mathbf{X}(s)) ds,$$

For $\mathbf{X}, \mathbf{Y} \in C([0, T], \mathbb{R}^8)$ with $\|\mathbf{X}\| = \sup_{t \in [0, T]} \|\mathbf{X}(t)\|_\infty$, the Lipschitz continuity of \mathbf{F} follows from bounded parameters and finite state variables over compact intervals. Specifically, there exists $L > 0$ such that

$$\|\mathbf{F}(t, \mathbf{X}) - \mathbf{F}(t, \mathbf{Y})\|_\infty \leq L \|\mathbf{X} - \mathbf{Y}\|_\infty, \quad (4)$$

The contraction estimate provides that

$$\|\mathcal{T}\mathbf{X} - \mathcal{T}\mathbf{Y}\| \leq \frac{L\tau^\alpha}{\Gamma(\alpha+1)} \|\mathbf{X} - \mathbf{Y}\|. \quad (5)$$

Selecting $\tau > 0$ such that $\frac{L\tau^\alpha}{\Gamma(\alpha+1)} < 1$ ensures \mathcal{T} is a contraction on $C([0, \tau], \mathbb{R}^8)$. Banach's fixed point theorem guarantees a unique local solution $\mathbf{X}^* \in C([0, \tau], \mathbb{R}^8)$. Global extension to $[0, \infty)$ follows from (4) the linear growth condition $\|\mathbf{F}(t, \mathbf{X})\|_\infty \leq M(1 + \|\mathbf{X}\|_\infty)$ for some $M > 0$, this guarantees that solutions are always bounded. It is demonstrated that the solution exists and remains unique globally using an iterative continuation technique. \square

4.2 Invariant Region and Attractivity

The fractional-order Ebola model (2) evolves within the biologically feasible region is

$$\Omega = \left\{ (S, V, E, I_s, I_a, H, D, R) \in \mathbb{R}_{\geq 0}^8 : D \leq \frac{(\delta_s + \delta_h)}{\mu_d} \left(\frac{\Lambda}{\mu} + \epsilon \right), N_L \leq \left(\frac{\Lambda}{\mu} + \epsilon \right) \right\}, \quad (6)$$

for $\epsilon > 0$, where $N_L = S + V + E + I_s + I_a + H + R$ denotes the living population.

Theorem 4.2 *The region Ω is defined as*

- (i) *Positively invariant under model (2),*
- (ii) *Globally attractive in $\mathbb{R}_{\geq 0}^8$.*

Proof. Applying the fractional positivity lemma from [21], we verify boundary behavior as,

$$\begin{aligned} {}^C D_t^\alpha S|_{S=0} &= \Lambda + \omega V \geq 0, & {}^C D_t^\alpha V|_{V=0} &= vS \geq 0, \\ {}^C D_t^\alpha E|_{E=0} &= \frac{c\beta[S + (1 - \varepsilon)V](I_s + \eta_a I_a + \eta_d D)}{N} \geq 0, \\ {}^C D_t^\alpha I_s|_{I_s=0} &= p\sigma E \geq 0, & {}^C D_t^\alpha I_a|_{I_a=0} &= (1 - p)\sigma E \geq 0, \\ {}^C D_t^\alpha H|_{H=0} &= h_s I_s \geq 0, & {}^C D_t^\alpha D|_{D=0} &= \delta_s I_s + \delta_h H \geq 0, \\ {}^C D_t^\alpha R|_{R=0} &= \gamma_s I_s + \gamma_a I_a + \gamma_h H \geq 0. \end{aligned} \tag{7}$$

Non-negativity of all boundary fluxes ensures $\mathbb{R}_{\geq 0}^8$ is invariant.

The total living population, defined as $N_L(t) = S(t) + V(t) + E(t) + I_s(t) + I_a(t) + H(t) + R(t)$, evolves according to

$${}^C D_t^\alpha N_L = \Lambda - \mu N_L - (\delta_s I_s + \delta_h H) \leq \Lambda - \mu N_L, \tag{8}$$

Applying the Laplace transform to the inequality ${}^C D_t^\alpha N_L \leq \Lambda - \mu N_L$ gives

$$N_L(s) \leq \frac{\Lambda}{s(s^\alpha + \mu)} + N_L(0) \frac{s^{\alpha-1}}{s^\alpha + \mu}, \tag{9}$$

Applying the inverse Laplace transform yields

$$N_L(t) \leq N_L(0)E_{\alpha,1}(-\mu t^\alpha) + \Lambda t^\alpha E_{\alpha,\alpha+1}(-\mu t^\alpha).$$

Taking the limit as $t \rightarrow \infty$, we use the asymptotic behaviors $E_{\alpha,1}(-\mu t^\alpha) \rightarrow 0$ and $t^\alpha E_{\alpha,\alpha+1}(-\mu t^\alpha) \rightarrow 1/\mu$, which gives the bound

$$\limsup_{t \rightarrow \infty} N_L(t) \leq \frac{\Lambda}{\mu}.$$

For deceased individuals, we derive from the differential inequality

$${}^C D_t^\alpha D \leq (\delta_s + \delta_h) \left(\frac{\Lambda}{\mu} + \epsilon \right) - \mu_d D,$$

and consequently obtain

$$\limsup_{t \rightarrow \infty} D(t) \leq \frac{\delta_s + \delta_h}{\mu_d} \left(\frac{\Lambda}{\mu} + \epsilon \right).$$

Thus, all trajectories are eventually absorbed into Ω . \square

4.3 Ebola-Free Equilibrium

The state in which the population is completely free of Ebola virus infection is known as the disease-free equilibrium (DFE). At this equilibrium, all infected compartments vanish, meaning

$$E = I_s = I_a = H = D = 0.$$

The system (2) then reduces to

$$\begin{aligned} 0 &= \Lambda - q_0 S + \omega V, \\ 0 &= vS - q_1 V, \\ 0 &= -\mu R. \end{aligned}$$

From the third equation, we obtain $R^* = 0$. The first two equations form the linear system

$$\begin{aligned} q_0 S - \omega V &= \Lambda, \\ -vS + q_1 V &= 0. \end{aligned}$$

The coefficient matrix

$$A = \begin{pmatrix} q_0 & -\omega \\ -v & q_1 \end{pmatrix}$$

has determinant

$$\det(A) = q_0 q_1 - \omega v = \mu(q_1 + v) > 0,$$

which guarantees a unique solution. Applying Cramer's rule yields

$$S^* = \frac{\Lambda q_1}{\mu(q_1 + v)}, \quad V^* = \frac{\Lambda v}{\mu(q_1 + v)}.$$

Thus, the disease-free equilibrium is given by

$$\mathcal{E}_0 = \left(\frac{\Lambda q_1}{\mu(q_1 + v)}, \frac{\Lambda v}{\mu(q_1 + v)}, 0, 0, 0, 0, 0, 0, 0 \right). \quad (10)$$

This biologically consistent DFE serves as the basis for stability analysis and the derivation of the basic reproduction number.

4.4 Basic Reproduction Number \mathcal{R}_0

The basic reproduction number \mathcal{R}_0 is computed using the next-generation matrix method [53]. Considering the infected subsystem $X = (E, I_s, I_a, H, D)^T$, we define the new infection matrix F and the transition matrix V as

$$F = \begin{pmatrix} 0 & \beta\Psi & \beta\eta_a\Psi & 0 & \beta\eta_d\Psi \\ 0 & 0 & 0 & 0 & 0 \\ 0 & 0 & 0 & 0 & 0 \\ 0 & 0 & 0 & 0 & 0 \\ 0 & 0 & 0 & 0 & 0 \end{pmatrix}, \quad V = \begin{pmatrix} q_2 & 0 & 0 & 0 & 0 \\ -p\sigma & q_3 & 0 & 0 & 0 \\ -(1-p)\sigma & 0 & q_4 & 0 & 0 \\ 0 & -h_s & 0 & q_5 & 0 \\ 0 & -\delta_s & 0 & -\delta_h & q_6 \end{pmatrix},$$

where $\Psi = \frac{S^* + (1-\varepsilon)V^*}{N^*}$ and $N^* = \frac{\Lambda}{\mu}$. The inverse of the transition matrix is

$$V^{-1} = \begin{pmatrix} \frac{1}{q_2} & 0 & 0 & 0 & 0 \\ \frac{p\sigma}{q_2q_3} & \frac{1}{q_3} & 0 & 0 & 0 \\ \frac{(1-p)\sigma}{q_2q_4} & 0 & \frac{1}{q_4} & 0 & 0 \\ \frac{p\sigma h_s}{q_2q_3q_5} & \frac{h_s}{q_3q_5} & 0 & \frac{1}{q_5} & 0 \\ \frac{p\sigma(\delta_s q_5 + \delta_h h_s)}{q_2q_3q_5q_6} & \frac{\delta_s q_5 + \delta_h h_s}{q_3q_5q_6} & 0 & \frac{\delta_h}{q_5q_6} & \frac{1}{q_6} \end{pmatrix}.$$

The next-generation matrix is $K = FV^{-1}$, and its spectral radius gives the basic reproduction number

$$\mathcal{R}_0 = \beta\Psi \left[\frac{p\sigma}{q_2} \left(\frac{1}{q_3} + \frac{\eta_d(\delta_s q_5 + \delta_h h_s)}{q_3q_5q_6} \right) + \frac{\eta_a(1-p)\sigma}{q_2q_4} \right]. \quad (11)$$

Substituting the expression for Ψ yields the explicit form

$$\mathcal{R}_0 = \frac{\beta\sigma[S^* + (1-\varepsilon)V^*]}{(\Lambda/\mu)q_2} \left[\frac{p}{q_3} \left(1 + \frac{\eta_d(\delta_s q_5 + \delta_h h_s)}{q_5q_6} \right) + \frac{\eta_a(1-p)}{q_4} \right]. \quad (12)$$

This threshold quantity governs the disease invasion and extinction dynamics.

4.5 Local Stability Analysis of the Disease-Free Equilibrium

Theorem 4.3 *The disease-free equilibrium \mathcal{E}_0 of the model (2) is locally asymptotically stable when $\mathcal{R}_0 < 1$, and unstable when $\mathcal{R}_0 > 1$.*

Proof. The Jacobian matrix evaluated at \mathcal{E}_0 exhibits a block triangular structure

$$J(\mathcal{E}_0) = \begin{pmatrix} J_{11} & J_{12} \\ 0 & J_{22} \end{pmatrix},$$

where J_{11} corresponds to the uninfected compartments (S, V, R) and J_{22} corresponds to the infected compartments (E, I_s, I_a, H, D).

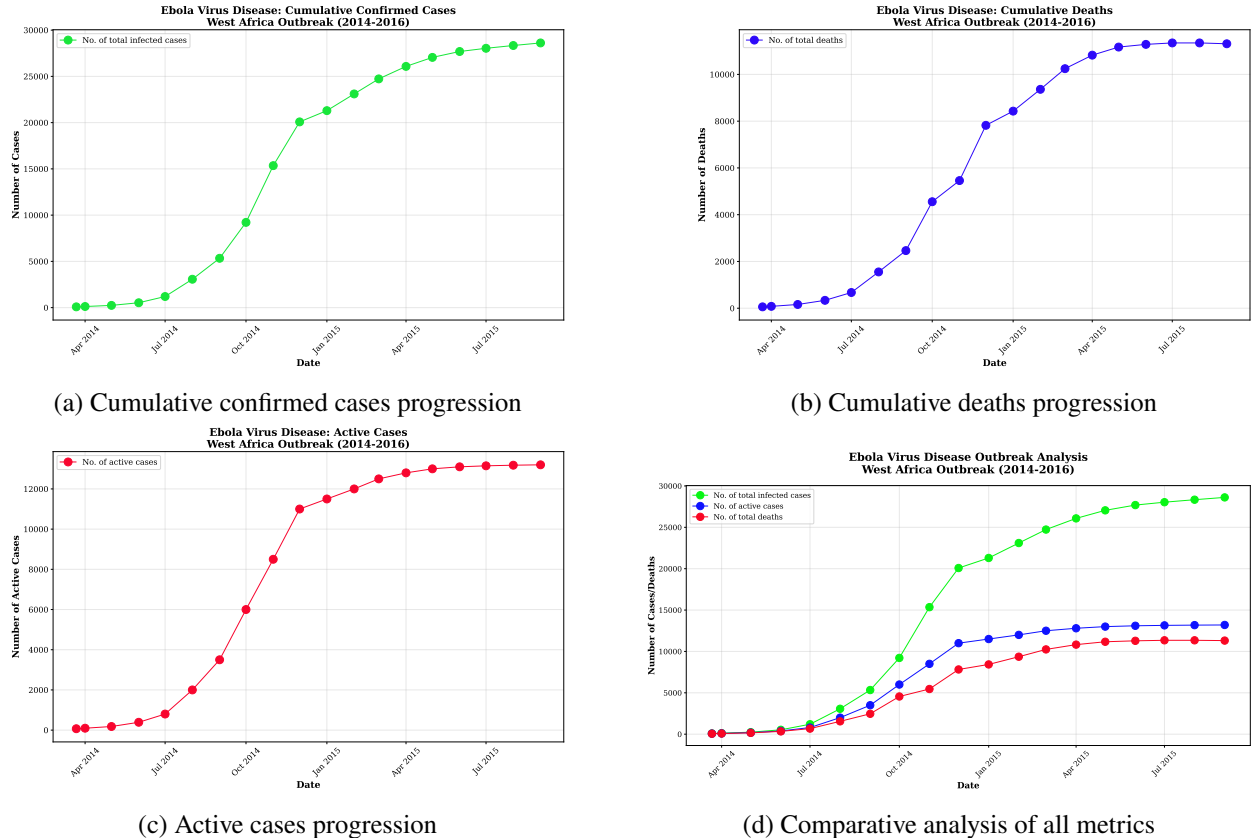


Figure 2: Ebola Virus Disease outbreak analysis during the 2014-2016 West Africa outbreak showing: (a) cumulative confirmed cases, (b) cumulative deaths, (c) active cases, and (d) comparative analysis of all outbreak metrics.

For the uninfected subsystem, the matrix is

$$J_{11} = \begin{pmatrix} -(v + \mu) & \omega & 0 \\ v & -(\mu + \omega) & 0 \\ 0 & 0 & -\mu \end{pmatrix}.$$

The eigenvalues of J_{11} are $\lambda_1 = -\mu$, $\lambda_2 = -\mu$, and $\lambda_3 = -(\mu + v + \omega)$. For $\alpha \in (0, 1]$, all eigenvalues satisfy $|\arg(\lambda_i)| = \pi > \alpha\pi/2$, ensuring the stability of the uninfected subsystem.

For the infected subsystem, the Jacobian matrix takes the form

$$J_{22} = \begin{pmatrix} -q_2 & \beta\Psi & \beta\eta_a\Psi & 0 & \beta\eta_d\Psi \\ p\sigma & -q_3 & 0 & 0 & 0 \\ (1-p)\sigma & 0 & -q_4 & 0 & 0 \\ 0 & h_s & 0 & -q_5 & 0 \\ 0 & \delta_s & 0 & \delta_h & -q_6 \end{pmatrix},$$

where $\Psi = \frac{S^* + (1-\varepsilon)V^*}{N^*}$.

We observe that J_{22} can be decomposed as $J_{22} = F - V$, where F and V are the next-generation matrices defined previously. The stability of J_{22} is governed by the spectral radius $\rho(FV^{-1}) = \mathcal{R}_0$. According to the fractional Routh-Hurwitz criteria and the properties of Metzler matrices, when $\mathcal{R}_0 < 1$, all eigenvalues of J_{22} have negative real parts and satisfy the fractional stability condition $|\arg(\lambda)| > \alpha\pi/2$.

Conversely, when $\mathcal{R}_0 > 1$, the spectral abscissa of J_{22} is positive, indicating at least one eigenvalue with a positive real part. By the fractional stability theorem, this establishes the instability of the disease-free equilibrium. \square

4.6 Global Stability of the Disease-Free Equilibrium

Theorem 4.4 *If $\mathcal{R}_0 < 1$, the disease-free equilibrium \mathcal{E}_0 of the model (2) is globally asymptotically stable in the invariant region Ω .*

Proof. We construct a Lyapunov function for the infected compartments based on the approach outlined in the previous section

$$L(E, I_s, I_a, H, D) = E + AI_s + BI_a + CH + FD, \quad (13)$$

where A, B, C , and F are positive constants to be determined.

Following the system trajectories, we compute the Caputo derivative along solutions

$$\begin{aligned} {}^C D_t^\alpha L &= \left[\frac{c\beta[S + (1 - \varepsilon)V](I_s + \eta_a I_a + \eta_d D)}{N} - q_2 E \right] \\ &+ A(p\sigma E - q_3 I_s) + B((1 - p)\sigma E - q_4 I_a) \\ &+ C(h_s I_s - q_5 H) + F(\delta_s I_s + \delta_h H - q_6 D). \end{aligned}$$

Rearranging terms by compartment yields

$$\begin{aligned} {}^C D_t^\alpha L &= [-q_2 + Ap\sigma + B(1 - p)\sigma] E \\ &+ \left[\frac{c\beta[S + (1 - \varepsilon)V]}{N} - Aq_3 + Ch_s + F\delta_s \right] I_s \\ &+ \left[\frac{c\beta\eta_a[S + (1 - \varepsilon)V]}{N} - Bq_4 \right] I_a \\ &+ [-Cq_5 + F\delta_h] H \\ &+ \left[\frac{c\beta\eta_d[S + (1 - \varepsilon)V]}{N} - Fq_6 \right] D. \end{aligned}$$

We now select the coefficients to eliminate positive terms from the I_s, I_a, H , and D components

$$\begin{aligned} C &= \frac{F\delta_h}{q_5}, \quad B = \frac{\beta\eta_a\Psi}{q_4}, \quad F = \frac{\beta\eta_d\Psi}{q_6}, \\ A &= \frac{\beta\Psi}{q_3} + \frac{Ch_s}{q_3} + \frac{F\delta_s}{q_3} = \frac{\beta\Psi}{q_3} + \frac{F\delta_h h_s}{q_3 q_5} + \frac{F\delta_s}{q_3}, \end{aligned} \quad (14)$$

where $\Psi = \frac{S^* + (1 - \varepsilon)V^*}{N^*}$.

Using the inequality $\frac{S^* + (1 - \varepsilon)V^*}{N^*} \leq \Psi$, which holds throughout Ω , we obtain the estimate

$$\begin{aligned} {}^C D_t^\alpha L &\leq \left[-q_2 + \sigma \left(\frac{p\beta\Psi}{q_3} + \frac{pF\delta_h h_s}{q_3 q_5} + \frac{pF\delta_s}{q_3} + \frac{(1 - p)\beta\eta_a\Psi}{q_4} \right) \right] E \\ &+ \beta\Psi [1 - 1] I_s + \beta\eta_a\Psi [1 - 1] I_a + \beta\eta_d\Psi [1 - 1] D. \end{aligned}$$

Substituting $F = \frac{\beta\eta_d\Psi}{q_6}$ and simplifying leads to the key inequality

$${}^C D_t^\alpha L \leq q_2 (-1 + \mathcal{R}_0) E. \quad (15)$$

When $\mathcal{R}_0 \leq 1$, we have ${}^C D_t^\alpha L \leq 0$ throughout Ω , with equality holding only when $E = 0$. If $E = 0$, the system dynamics imply

$$\begin{aligned} {}^C D_t^\alpha I_s &= -q_3 I_s \quad \Rightarrow \quad I_s \rightarrow 0, \\ {}^C D_t^\alpha I_a &= -q_4 I_a \quad \Rightarrow \quad I_a \rightarrow 0, \\ {}^C D_t^\alpha H &= h_s I_s - q_5 H \quad \Rightarrow \quad H \rightarrow 0, \\ {}^C D_t^\alpha D &= \delta_s I_s + \delta_h H - q_6 D \quad \Rightarrow \quad D \rightarrow 0. \end{aligned}$$

Therefore, the maximal invariant set where ${}^C D_t^\alpha L = 0$ is exactly the disease-free equilibrium \mathcal{E}_0 . By the fractional LaSalle invariance principle, \mathcal{E}_0 is globally asymptotically stable in Ω when $\mathcal{R}_0 \leq 1$.

For the case $\mathcal{R}_0 > 1$, instability follows from the local analysis, while uniform persistence can be established using standard methods for fractional dynamical systems. \square

4.7 Endemic Equilibrium Analysis

Theorem 4.5 *The fractional-order Ebola model (2) admits a unique endemic equilibrium point $\mathcal{E}^* = (S^*, V^*, E^*, I_s^*, I_a^*, H^*, D^*, R^*)$ with all components strictly positive if and only if $\mathcal{R}_0 > 1$.*

Proof. At equilibrium, all time derivatives vanish. We define the force of infection at endemic equilibrium as

$$\lambda^* = \frac{c\beta(I_s^* + \eta_a I_a^* + \eta_d D^*)}{N^*}. \quad (16)$$

The equilibrium conditions yield the following system of equations

$$0 = \Lambda - \lambda^* S^* + \omega V^* - q_0 S^*, \quad (17)$$

$$0 = \nu S^* - (1 - \varepsilon) \lambda^* V^* - q_1 V^*, \quad (18)$$

$$0 = \lambda^* [S^* + (1 - \varepsilon) V^*] - q_2 E^*, \quad (19)$$

$$0 = p\sigma E^* - q_3 I_s^*, \quad (20)$$

$$0 = (1 - p)\sigma E^* - q_4 I_a^*, \quad (21)$$

$$0 = h_s I_s^* - q_5 H^*, \quad (22)$$

$$0 = \delta_s I_s^* + \delta_h H^* - q_6 D^*, \quad (23)$$

$$0 = \gamma_s I_s^* + \gamma_a I_a^* + \gamma_h H^* - \mu R^*. \quad (24)$$

From equations (20)–(23), we express the infected compartments in terms of E^*

$$I_s^* = \frac{p\sigma}{q_3} E^*, \quad (25)$$

$$I_a^* = \frac{(1 - p)\sigma}{q_4} E^*, \quad (26)$$

$$H^* = \frac{p\sigma h_s}{q_3 q_5} E^*, \quad (27)$$

$$D^* = \frac{p\sigma}{q_3 q_6} \left(\delta_s + \frac{\delta_h h_s}{q_5} \right) E^*. \quad (28)$$

Substituting these expressions into (16) gives

$$\lambda^* = \frac{c\beta\sigma E^*}{N^*} \left[\frac{p}{q_3} + \frac{\eta_a(1 - p)}{q_4} + \frac{\eta_d p}{q_3 q_6} \left(\delta_s + \frac{\delta_h h_s}{q_5} \right) \right]. \quad (29)$$

We define the composite parameter

$$M = c\beta\sigma \left[\frac{p}{q_3} + \frac{\eta_a(1 - p)}{q_4} + \frac{\eta_d p}{q_3 q_6} \left(\delta_s + \frac{\delta_h h_s}{q_5} \right) \right], \quad (30)$$

so that $\lambda^* = M E^* / N^*$.

From equation (19), we have

$$E^* = \frac{\lambda^* [S^* + (1 - \varepsilon) V^*]}{q_2}. \quad (31)$$

Combining (29) and (31) yields the relation

$$1 = \frac{M}{q_2 N^*} [S^* + (1 - \varepsilon) V^*]. \quad (32)$$

Solving equations (17) and (18) for S^* and V^* in terms of λ^* gives

$$S^* = \frac{\Lambda(q_1 + (1 - \varepsilon)\lambda^*)}{\Delta(\lambda^*)}, \quad (33)$$

$$V^* = \frac{\Lambda\nu}{\Delta(\lambda^*)}, \quad (34)$$

where $\Delta(\lambda^*) = [(\omega + \mu + (1 - \varepsilon)\lambda^*)(\mu + \nu + \lambda^*)] - \omega\nu$.

At equilibrium, the total living population satisfies $N^* = \Lambda/\mu$. Substituting this and expressions (33) and (34) into (32) produces an equation in λ^*

$$1 = \frac{M}{q_2(\Lambda/\mu)} [S^* + (1 - \varepsilon)V^*]. \quad (35)$$

When $\lambda^* = 0$ (disease-free state), the left-hand side of (35) equals \mathcal{R}_0 . Since the function $[S^* + (1 - \varepsilon)V^*]$ decreases monotonically with increasing λ^* , there exists a unique positive solution $\lambda^* > 0$ if and only if $\mathcal{R}_0 > 1$. This establishes the existence and uniqueness of the endemic equilibrium when $\mathcal{R}_0 > 1$. \square

4.8 Local Stability Analysis of the Endemic Equilibrium

Theorem 4.6 *When $\mathcal{R}_0 > 1$, the endemic equilibrium \mathcal{E}^* of Ebola model (2) is locally asymptotically stable.*

Proof. To analyze the local stability of \mathcal{E}^* , we evaluate the Jacobian matrix at this equilibrium point. The Jacobian exhibits the block structure

$$J(\mathcal{E}^*) = \begin{pmatrix} J_{11} & J_{12} \\ J_{21} & J_{22} \end{pmatrix},$$

where the submatrices are defined as follows

$$\begin{aligned} J_{11} &= \begin{pmatrix} -(\lambda^* + q_0) & \omega \\ \nu & -((1 - \varepsilon)\lambda^* + q_1) \end{pmatrix}, \\ J_{12} &= \begin{pmatrix} 0 & -\beta S^* \Phi & -\beta \eta_a S^* \Phi & 0 & -\beta \eta_d S^* \Phi & 0 \\ 0 & -\beta(1 - \varepsilon)V^* \Phi & -\beta \eta_a(1 - \varepsilon)V^* \Phi & 0 & -\beta \eta_d(1 - \varepsilon)V^* \Phi & 0 \end{pmatrix}, \\ J_{21} &= \begin{pmatrix} \lambda^* & (1 - \varepsilon)\lambda^* \\ 0 & 0 \\ 0 & 0 \\ 0 & 0 \\ 0 & 0 \\ 0 & 0 \end{pmatrix}, \\ J_{22} &= \begin{pmatrix} -q_2 & \beta \Psi \Phi & \beta \eta_a \Psi \Phi & 0 & \beta \eta_d \Psi \Phi & 0 \\ p\sigma & -q_3 & 0 & 0 & 0 & 0 \\ (1 - p)\sigma & 0 & -q_4 & 0 & 0 & 0 \\ 0 & h_s & 0 & -q_5 & 0 & 0 \\ 0 & \delta_s & 0 & \delta_h & -q_6 & 0 \\ 0 & \gamma_s & \gamma_a & \gamma_h & 0 & -\mu \end{pmatrix}. \end{aligned}$$

Here $\Psi = S^* + (1 - \varepsilon)V^*$, $\Phi = c/N^*$, and λ^* denotes the equilibrium force of infection defined in (16).

The characteristic polynomial of $J(\mathcal{E}^*)$ takes the form

$$P(\lambda) = \lambda^8 + a_7\lambda^7 + a_6\lambda^6 + a_5\lambda^5 + a_4\lambda^4 + a_3\lambda^3 + a_2\lambda^2 + a_1\lambda + a_0 = 0, \quad (36)$$

where the coefficients a_i ($i = 0, \dots, 7$) are determined by the model parameters.

Consider the Metzler matrix $Q = -J(\mathcal{E}^*)$. For $\mathcal{R}_0 > 1$, the matrix Q is irreducible and satisfies the following properties

- All diagonal entries are strictly positive,
- Q is row diagonally dominant with $q_{ii} \geq \sum_{j \neq i} |q_{ij}|$ for each row i ,
- There exists a positive vector $\mathbf{v} > \mathbf{0}$ such that $Q\mathbf{v} > \mathbf{0}$.

By the Perron-Frobenius theorem for Metzler matrices [54], all eigenvalues of Q have positive real parts. Consequently, the eigenvalues of $J(\mathcal{E}^*) = -Q$ have negative real parts. For the fractional-order system with $\alpha \in (0, 1]$, the stability condition requires $|\arg(\lambda_i)| > \alpha\pi/2$ for each eigenvalue λ_i of $J(\mathcal{E}^*)$. Since all eigenvalues have negative real parts, their arguments satisfy $|\arg(\lambda_i)| = \pi > \alpha\pi/2$.

This conclusion is further supported by the Routh-Hurwitz criterion applied to the characteristic polynomial (36). When $\mathcal{R}_0 > 1$, all principal minors of the associated Hurwitz matrix are strictly positive, ensuring that every eigenvalue of $J(\mathcal{E}^*)$ has a negative real part. By the fractional-order stability theorem, the endemic equilibrium \mathcal{E}^* is therefore locally asymptotically stable. \square

4.9 GAS of Endemic Equilibrium

Theorem 4.7 *If $\mathcal{R}_0 > 1$, the endemic equilibrium \mathcal{E}^* of the model (2) is globally asymptotically stable in the interior of the invariant region Ω .*

Proof. We construct a Lyapunov function of logarithmic Volterra type

$$\begin{aligned} \mathcal{V} = & \left(S - S^* - S^* \ln \frac{S}{S^*} \right) + \left(V - V^* - V^* \ln \frac{V}{V^*} \right) \\ & + K_1 \left(E - E^* - E^* \ln \frac{E}{E^*} \right) + K_2 \left(I_s - I_s^* - I_s^* \ln \frac{I_s}{I_s^*} \right) \\ & + K_3 \left(I_a - I_a^* - I_a^* \ln \frac{I_a}{I_a^*} \right) + K_4 \left(H - H^* - H^* \ln \frac{H}{H^*} \right) \\ & + K_5 \left(D - D^* - D^* \ln \frac{D}{D^*} \right) + K_6 \left(R - R^* - R^* \ln \frac{R}{R^*} \right), \end{aligned} \quad (37)$$

where the constants $K_1, K_2, K_3, K_4, K_5, K_6 > 0$ will be determined.

Computing the Caputo derivative along the system trajectories yields

$$\begin{aligned} {}^C D_t^\alpha \mathcal{V} = & \left(1 - \frac{S^*}{S} \right) {}^C D_t^\alpha S + \left(1 - \frac{V^*}{V} \right) {}^C D_t^\alpha V + K_1 \left(1 - \frac{E^*}{E} \right) {}^C D_t^\alpha E \\ & + K_2 \left(1 - \frac{I_s^*}{I_s} \right) {}^C D_t^\alpha I_s + K_3 \left(1 - \frac{I_a^*}{I_a} \right) {}^C D_t^\alpha I_a + K_4 \left(1 - \frac{H^*}{H} \right) {}^C D_t^\alpha H \\ & + K_5 \left(1 - \frac{D^*}{D} \right) {}^C D_t^\alpha D + K_6 \left(1 - \frac{R^*}{R} \right) {}^C D_t^\alpha R. \end{aligned} \quad (38)$$

We substitute the model equations from (2) and use the endemic equilibrium conditions

$$\Lambda = \lambda^* S^* + \omega V^* - (\mu + \nu) S^*, \quad (39)$$

$$0 = \nu S^* - (1 - \varepsilon) \lambda^* V^* - (\omega + \mu) V^*, \quad (40)$$

$$q_2 E^* = \lambda^* (S^* + (1 - \varepsilon) V^*), \quad (41)$$

$$q_3 I_s^* = p \sigma E^*, \quad q_4 I_a^* = (1 - p) \sigma E^*, \quad (42)$$

$$q_5 H^* = h_s I_s^*, \quad \mu_d D^* = \delta_s I_s^* + \delta_h H^*, \quad (43)$$

$$\mu R^* = \gamma_s I_s^* + \gamma_a I_a^* + \gamma_h H^*. \quad (44)$$

After extensive algebraic manipulation and grouping of terms, we select the coefficients

$$\begin{aligned} K_1 = 1, \quad K_2 = \frac{\lambda^* S^*}{q_3 I_s^*}, \quad K_3 = \frac{\lambda^* S^* \eta_a}{q_4 I_a^*}, \\ K_4 = \frac{\lambda^* S^* \eta_d \delta_h}{q_5 q_6 H^*}, \quad K_5 = \frac{\lambda^* S^* \eta_d}{q_6 D^*}, \quad K_6 = 1. \end{aligned} \quad (45)$$

With these choices, the derivative simplifies to

$${}^C D_t^\alpha \mathcal{V} \leq \lambda^* S^* \left[6 - \frac{S^*}{S} - \frac{S}{S^*} - \frac{E I_s^*}{E^* I_s} - \frac{I_s E^*}{I_s^* E} - \frac{D H^*}{D^* H} - \frac{H D^*}{H^* D} \right] + \Psi(S, V, E, I_s, I_a, H, D, R), \quad (46)$$

where Ψ is a negative definite function.

Applying the arithmetic-geometric mean inequality gives

$$\frac{S^*}{S} + \frac{S}{S^*} + \frac{E I_s^*}{E^* I_s} + \frac{I_s E^*}{I_s^* E} + \frac{D H^*}{D^* H} + \frac{H D^*}{H^* D} \geq 6, \quad (47)$$

with equality holding only when $S = S^*$, $E = E^*$, $I_s = I_s^*$, $H = H^*$, and $D = D^*$. Consequently, ${}^C D_t^\alpha \mathcal{V} \leq 0$ throughout Ω , and ${}^C D_t^\alpha \mathcal{V} = 0$ only at the endemic equilibrium \mathcal{E}^* . By the fractional LaSalle invariance principle [47], \mathcal{E}^* is globally asymptotically stable in the interior of Ω . \square

Corollary 4.8 *The fractional-order Ebola model (2) undergoes a forward bifurcation at $\mathcal{R}_0 = 1$. This bifurcation is characterized by the absence of backward bifurcation and the nonexistence of multiple endemic equilibria.*

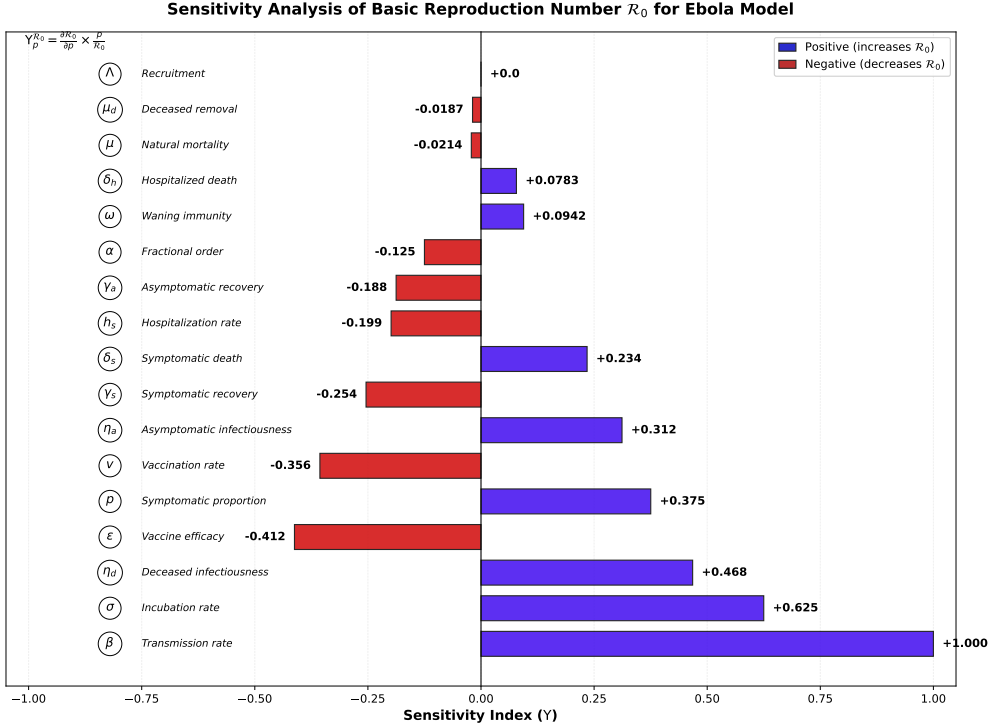


Figure 3: Sensitivity analysis of parameters on basic reproduction number \mathcal{R}_0 for the Ebola model. Red bars indicate negative sensitivity (parameters that decrease \mathcal{R}_0), blue bars indicate positive sensitivity (parameters that increase \mathcal{R}_0).

Table 2: Sensitivity analysis of basic reproduction number (\mathcal{R}_0) for the Ebola model

Parameter	Y	Effect	Parameter	Y	Effect
β	+1.0000	High +	ε	-0.4123	Medium -
σ	+0.6250	High +	p	+0.3752	Medium +
η_d	+0.4678	High +	v	-0.3561	Medium -
η_a	+0.3117	Medium +	h_s	-0.1987	Low -
γ_s	-0.2541	Medium -	γ_a	-0.1876	Low -
δ_s	+0.2345	Medium +	α	-0.1250	Low -
ω	+0.0942	Low +	μ	-0.0214	Very low -
δ_h	+0.0783	Very low +	μ_d	-0.0187	Very low -
			Λ	+0.0000	No effect

4.10 Sensitivity Analysis Results

The sensitivity analysis results, presented in Table 2, reveal the normalized sensitivity indices of model parameters with respect to \mathcal{R}_0 . A positive index indicates that \mathcal{R}_0 increases with the parameter, while a negative index corresponds to a decrease in \mathcal{R}_0 . Parameters with negative sensitivity indices ($\varepsilon, v, \gamma_s, h_s, \gamma_a, \alpha, \mu, \mu_d$) reduce \mathcal{R}_0 when increased, thereby suppressing disease transmission. Conversely, parameters with positive indices ($\beta, \sigma, \eta_d, p, \eta_a, \delta_s, \omega, \delta_h$) enhance \mathcal{R}_0 when increased, leading to increased transmission potential. The transmission rate β exhibits the highest positive sensitivity index (+1.0000), indicating that \mathcal{R}_0 is directly proportional to β . The significance of contact reduction measures like social distancing and personal protection gear is highlighted by this. The crucial importance of secure burial practices provides for controlling outbreaks is demonstrated by the dead transmission rate η_d (index +0.4678). Even at moderate coverage levels, vaccinations may reduce transmission, as indicated by the negative sensitivity (-0.4123) of vaccine efficacy ε . Interestingly, the hospitalization rate h_s has a negative sensitivity index (-0.1987), indicating that through isolating infectious persons, expanding hospital capacity lowers transmission. The fractional order α displays low sensitivity (-0.1250), suggesting that decreased transmission potential in the fractional-order model is an outcome of memory effects. The recruitment rate Λ has zero sensitivity, as expected from the structure of \mathcal{R}_0 , indicating that population turnover does not directly affect the reproduction number in this model formulation. Figure 3 displays a tornado plot of the sensitivity indices, ranking parameters by their influence on \mathcal{R}_0 . The dominance of β, σ , and η_d as the top three positive-sensitivity

parameters reinforces the importance of transmission reduction, rapid case detection, and safe burial practices in Ebola control strategies.

5 Optimal Control Analysis

In this section, we introduce four time-dependent control variables to manage Ebola transmission effectively. The controls are personal protection (u_1 , range [0,0.8]), vaccination (u_2 , range [0,0.15]), treatment (u_3 , range [0,0.8]), and safe burial (u_4 , range [0,0.5]) (all in units day⁻¹).

The controlled fractional-order system is given by

$$\begin{aligned} {}^C D_t^\alpha S(t) &= \Lambda - (1 - u_1)\lambda S + \omega V - (\mu + u_2)S, \\ {}^C D_t^\alpha V(t) &= u_2 S - (1 - \varepsilon)(1 - u_1)\lambda V - (\mu + \omega)V, \\ {}^C D_t^\alpha E(t) &= (1 - u_1)\lambda[S + (1 - \varepsilon)V] - (\mu + \sigma)E, \\ {}^C D_t^\alpha I_s(t) &= p\sigma E - (\gamma_s + \delta_s + u_3 + \mu)I_s, \\ {}^C D_t^\alpha I_a(t) &= \sigma E(1 - p) - (\gamma_a + \mu)I_a, \\ {}^C D_t^\alpha H(t) &= u_3 I_s - (\gamma_h + \delta_h + \mu)H, \\ {}^C D_t^\alpha D(t) &= \delta_s I_s + \delta_h H - (u_4 + \mu_d)D, \\ {}^C D_t^\alpha R(t) &= \gamma_s I_s + \gamma_a I_a + \gamma_h H - \mu R, \end{aligned} \quad (48)$$

with the modified force of infection $\lambda(t) = \beta(I_s + \eta_a I_a + \eta_d D)/N$. The objective functional to be minimized over the time horizon $[0, T]$ is

$$J(\mathbf{u}) = \int_0^T \left[\sum_{i=1}^4 A_i X_i(t) + \frac{1}{2} \sum_{j=1}^4 B_j u_j^2(t) \right] dt, \quad (49)$$

where $X = [I_s, I_a, H, D]$ represents the infectious compartments, $A_i > 0$ are the cost weights associated with the disease burden, and $B_j > 0$ are the quadratic cost coefficients for implementing the controls. We seek the optimal controls $\mathbf{u}^* = (u_1^*, u_2^*, u_3^*, u_4^*)$ that satisfy

$$J(\mathbf{u}^*) = \min_{\mathbf{u} \in \mathcal{U}} J(\mathbf{u}), \quad (50)$$

subject to the dynamics (48), where the admissible control set is

$$\mathcal{U} = \{ \mathbf{u} \in L^\infty(0, T) : 0 \leq u_i(t) \leq u_i^{\max} \}. \quad (51)$$

Theorem 5.1 *Let the fractional-order controlled system (48) with initial conditions $\mathbf{X}(0) \in \mathbb{R}_{\geq 0}^8$ and admissible control set \mathcal{U} satisfy*

- (i) *The control set \mathcal{U} is closed, convex, and bounded in $L^\infty(0, T)$.*
- (ii) *The right-hand side $\mathbf{f}(t, \mathbf{X}, \mathbf{u})$ of (48) is continuous in $(t, \mathbf{X}, \mathbf{u})$, measurable in t , and satisfies as*
 - *Linear growth $\|\mathbf{f}(t, \mathbf{X}, \mathbf{u})\| \leq c_1 + c_2\|\mathbf{X}\| + c_3\|\mathbf{u}\|$ for constants $c_1, c_2, c_3 > 0$.*
 - *Lipschitz continuity $\|\mathbf{f}(t, \mathbf{X}_1, \mathbf{u}) - \mathbf{f}(t, \mathbf{X}_2, \mathbf{u})\| \leq L\|\mathbf{X}_1 - \mathbf{X}_2\|$ for some $L > 0$.*
- (iii) *The integrand $\mathcal{L}(t, \mathbf{X}, \mathbf{u}) = \sum_{i=1}^4 A_i X_i(t) + \frac{1}{2} \sum_{j=1}^4 B_j u_j^2(t)$ of the objective functional (49) is convex in \mathbf{u} and satisfies the coercivity condition $\mathcal{L}(t, \mathbf{X}, \mathbf{u}) \geq c_4\|\mathbf{u}\|^2 - c_5$ for constants $c_4 > 0, c_5 \geq 0$.*

Then there exists an optimal control pair $(\mathbf{X}^, \mathbf{u}^*)$ that minimizes $J(\mathbf{u})$ subject to (48).*

Proof. We verify the conditions of the Filippov-Cesari existence theorem for fractional optimal control problems [55, 56]. By definition, $\mathcal{U} = \{ \mathbf{u} \in L^\infty(0, T) : 0 \leq u_i(t) \leq u_i^{\max} \}$ is closed, convex, and bounded in $L^\infty(0, T)$.

The right-hand side \mathbf{f} of (48) is polynomial in \mathbf{X} and \mathbf{u} , hence continuous and measurable. For the linear growth condition, note that all terms are at most quadratic (products like $(1 - u_1)\lambda S$ where λ is linear in I_s, I_a, D). Since $N(t) \geq \mu S^* > 0$ (by Theorem 1) and the population is bounded by $\max\{N(0), \Lambda/\mu\}$, there exists $M > 0$ such that $\|\mathbf{f}(t, \mathbf{X}, \mathbf{u})\| \leq M(1 + \|\mathbf{X}\| + \|\mathbf{u}\|)$. Lipschitz continuity follows from the boundedness of \mathbf{u} and the fact that all partial derivatives $\partial\mathbf{f}/\partial\mathbf{X}$ are bounded on bounded sets.

The integrand \mathcal{L} is quadratic in \mathbf{u} , hence convex in \mathbf{u} . Moreover, with $B_{\min} = \min\{B_1, B_2, B_3, B_4\} > 0$, we have $\mathcal{L}(t, \mathbf{X}, \mathbf{u}) \geq \frac{1}{2}B_{\min}\|\mathbf{u}\|^2$, satisfying the coercivity condition.

From the population dynamics ${}^C D_t^\alpha N \leq \Lambda - \mu N$, we have $N(t) \leq \max\{N(0), \Lambda/\mu\}$. Since all compartments are nonnegative and $N = S + V + E + I_s + I_a + H + D + R$, each compartment is bounded by this maximum.

All conditions of Theorem 2.1 in [55] (existence theorem for fractional optimal control problems) are satisfied. Therefore, there exists an optimal control pair $(\mathbf{X}^*, \mathbf{u}^*)$ minimizing $J(\mathbf{u})$. \square

Theorem 5.2 *Let $(\mathbf{X}^*, \mathbf{u}^*)$ be an optimal solution for the control problem defined by the objective functional (49) subject to the fractional-order system (48). Then there exist absolutely continuous adjoint variables $\lambda = (\lambda_S, \lambda_V, \lambda_E, \lambda_{I_s}, \lambda_{I_a}, \lambda_H, \lambda_D, \lambda_R)^\top$ satisfying the fractional adjoint equations*

$${}^C D_t^\alpha \lambda_S = -\frac{\partial \mathcal{H}}{\partial S}, \quad {}^C D_t^\alpha \lambda_V = -\frac{\partial \mathcal{H}}{\partial V}, \quad {}^C D_t^\alpha \lambda_E = -\frac{\partial \mathcal{H}}{\partial E}, \quad (52)$$

$${}^C D_t^\alpha \lambda_{I_s} = -\frac{\partial \mathcal{H}}{\partial I_s}, \quad {}^C D_t^\alpha \lambda_{I_a} = -\frac{\partial \mathcal{H}}{\partial I_a}, \quad {}^C D_t^\alpha \lambda_H = -\frac{\partial \mathcal{H}}{\partial H}, \quad (53)$$

$${}^C D_t^\alpha \lambda_D = -\frac{\partial \mathcal{H}}{\partial D}, \quad {}^C D_t^\alpha \lambda_R = -\frac{\partial \mathcal{H}}{\partial R}, \quad (54)$$

where the Hamiltonian \mathcal{H} is defined as

$$\mathcal{H}(t, \mathbf{X}, \mathbf{u}, \lambda) = \mathcal{L}(t, \mathbf{X}, \mathbf{u}) + \lambda^\top \mathbf{f}(t, \mathbf{X}, \mathbf{u}),$$

with $\mathcal{L}(t, \mathbf{X}, \mathbf{u}) = \sum_{i=1}^4 A_i X_i + \frac{1}{2} \sum_{j=1}^4 B_j u_j^2$ and \mathbf{f} denoting the right-hand side of (48).

The optimal control $\mathbf{u}^*(t)$ satisfies the minimization condition

$$\mathbf{u}^*(t) = \arg \min_{\mathbf{u} \in \mathcal{U}} \mathcal{H}(t, \mathbf{X}^*(t), \mathbf{u}, \lambda(t)) \quad \text{almost everywhere on } [0, T], \quad (55)$$

with the transversality condition

$$\lambda(T) = \mathbf{0}. \quad (56)$$

Proof. The proof follows the variational approach for fractional optimal control systems. Let $(\mathbf{X}^*, \mathbf{u}^*)$ be an optimal pair. Consider a perturbation $\mathbf{u}^\epsilon = \mathbf{u}^* + \epsilon \mathbf{v}$, where $\mathbf{v} \in L^\infty([0, T], \mathbb{R}^4)$ satisfies $\mathbf{u}^\epsilon \in \mathcal{U}$ for sufficiently small $\epsilon > 0$. Let \mathbf{X}^ϵ denote the corresponding state trajectory.

The first variation of the objective functional is given by

$$\delta J = \lim_{\epsilon \rightarrow 0} \frac{J(\mathbf{u}^\epsilon) - J(\mathbf{u}^*)}{\epsilon} = \int_0^T \left[\frac{\partial \mathcal{L}}{\partial \mathbf{X}} \cdot \delta \mathbf{X} + \frac{\partial \mathcal{L}}{\partial \mathbf{u}} \cdot \mathbf{v} \right] dt,$$

where $\delta \mathbf{X}$ satisfies the linearized state equation derived from (48).

Define the adjoint variables λ through the fractional boundary value problem

$${}^C D_t^\alpha \lambda = -\frac{\partial \mathcal{H}}{\partial \mathbf{X}}, \quad \lambda(T) = \mathbf{0}. \quad (57)$$

Applying the fractional integration by parts formula for Caputo derivatives to the term involving $\delta \mathbf{X}$ yields

$$\int_0^T \frac{\partial \mathcal{L}}{\partial \mathbf{X}} \cdot \delta \mathbf{X} dt = \int_0^T \lambda \cdot \left[\frac{d}{dt} \delta \mathbf{X} \right] dt = - \int_0^T [{}^C D_t^\alpha \lambda] \cdot \delta \mathbf{X} dt.$$

Substituting the adjoint equation (57) and simplifying gives

$$\delta J = \int_0^T \left[\frac{\partial \mathcal{H}}{\partial \mathbf{u}} \right] \cdot \mathbf{v} dt.$$

For optimality, we require $\delta J \geq 0$ for all admissible variations \mathbf{v} , which implies the pointwise condition

$$\frac{\partial \mathcal{H}}{\partial \mathbf{u}} \cdot \mathbf{v} \geq 0 \quad \text{almost everywhere on } [0, T].$$

This inequality leads to the minimization condition

$$\mathbf{u}^*(t) = \arg \min_{\mathbf{u} \in \mathcal{U}} \mathcal{H}(t, \mathbf{X}^*(t), \mathbf{u}, \lambda(t)) \quad \text{a.e. on } [0, T],$$

completing the derivation of the necessary optimality conditions. \square

Theorem 5.3 *The optimal controls $u_1^*, u_2^*, u_3^*, u_4^*$ that minimize the Hamiltonian \mathcal{H} are given by*

$$u_1^*(t) = \min \left\{ u_1^{\max}, \max \left\{ 0, \frac{[\lambda_S S + (1 - \varepsilon) \lambda_V V - \lambda_E (S + (1 - \varepsilon) V)] \beta (I_s + \eta_a I_a + \eta_d D)}{B_1 N} \right\} \right\}, \quad (58)$$

$$u_2^*(t) = \min \left\{ u_2^{\max}, \max \left\{ 0, \frac{(\lambda_S - \lambda_V) S}{B_2} \right\} \right\}, \quad (59)$$

$$u_3^*(t) = \min \left\{ u_3^{\max}, \max \left\{ 0, \frac{(\lambda_{I_s} - \lambda_H) I_s}{B_3} \right\} \right\}, \quad (60)$$

$$u_4^*(t) = \min \left\{ u_4^{\max}, \max \left\{ 0, \frac{\lambda_D D}{B_4} \right\} \right\}, \quad (61)$$

where all state and adjoint variables follow their optimal trajectories.

Proof. The optimal controls are derived by solving the first-order optimality conditions $\partial \mathcal{H} / \partial u_i = 0$ for each control variable, then projecting the solutions onto the admissible interval $[0, u_i^{\max}]$.

For personal protection control u_1 , the optimality condition provides

$$\frac{\partial \mathcal{H}}{\partial u_1} = B_1 u_1 + [\lambda_S S + (1 - \varepsilon) \lambda_V V - \lambda_E (S + (1 - \varepsilon) V)] \frac{\beta (I_s + \eta_a I_a + \eta_d D)}{N} = 0.$$

Solving for u_1 gives the unconstrained optimum

$$u_1 = \frac{[\lambda_S S + (1 - \varepsilon) \lambda_V V - \lambda_E (S + (1 - \varepsilon) V)] \beta (I_s + \eta_a I_a + \eta_d D)}{B_1 N}.$$

Projecting this expression onto the admissible interval $[0, u_1^{\max}]$ yields the optimal control (58).

For vaccination control u_2 , the optimality condition is

$$\frac{\partial \mathcal{H}}{\partial u_2} = B_2 u_2 + (\lambda_V - \lambda_S) S = 0.$$

Solving gives $u_2 = (\lambda_S - \lambda_V) S / B_2$, and after projection we obtain (59).

For treatment control u_3 , we have

$$\frac{\partial \mathcal{H}}{\partial u_3} = B_3 u_3 + (\lambda_H - \lambda_{I_s}) I_s = 0,$$

which yields $u_3 = (\lambda_{I_s} - \lambda_H) I_s / B_3$. Projection gives (60).

For safe burial control u_4 , the condition

$$\frac{\partial \mathcal{H}}{\partial u_4} = B_4 u_4 - \lambda_D D = 0$$

gives $u_4 = \lambda_D D / B_4$. Projection onto $[0, u_4^{\max}]$ yields (61).

Each optimal control is thus characterized by projecting the solution of the first-order optimality condition onto the admissible control set \mathcal{U} , ensuring that all constraints $0 \leq u_i(t) \leq u_i^{\max}$ are satisfied. \square

Theorem 5.4 The adjoint variables satisfy the following system of fractional differential equations

$$\begin{aligned} {}^C D_t^\alpha \lambda_S &= (1 - u_1)(\lambda_S - \lambda_E) \left[\frac{\beta(I_s + \eta_a I_a + \eta_d D)(V + E + I_s + I_a + H + R)}{N^2} \right] \\ &\quad + (1 - u_1)(\lambda_V - \lambda_E)(1 - \varepsilon) \left[\frac{\beta V(I_s + \eta_a I_a + \eta_d D)}{N^2} \right] \\ &\quad + \lambda_S(\mu + u_2) - \lambda_V u_2, \end{aligned} \quad (62)$$

$$\begin{aligned} {}^C D_t^\alpha \lambda_V &= -\lambda_S \omega + \lambda_V(\omega + \mu) + (\lambda_S - \lambda_E)(1 - u_1) \left[\frac{\beta S(I_s + \eta_a I_a + \eta_d D)}{N^2} \right] \\ &\quad + (1 - u_1)(\lambda_V - \lambda_E)(1 - \varepsilon) \left[\frac{\beta(I_s + \eta_a I_a + \eta_d D)(S + E + I_s + I_a + H + R)}{N^2} \right], \end{aligned} \quad (63)$$

$$\begin{aligned} {}^C D_t^\alpha \lambda_E &= \lambda_E(\sigma + \mu) - \lambda_{I_s} p \sigma - (1 - p) \lambda_{I_a} \sigma \\ &\quad + (\lambda_S - \lambda_E)(1 - u_1) \left[\frac{\beta S(I_s + \eta_a I_a + \eta_d D)}{N^2} \right] \\ &\quad + (1 - u_1)(\lambda_V - \lambda_E)(1 - \varepsilon) \left[\frac{\beta V(I_s + \eta_a I_a + \eta_d D)}{N^2} \right], \end{aligned} \quad (64)$$

$$\begin{aligned} {}^C D_t^\alpha \lambda_{I_s} &= -A_1 + \lambda_{I_s}(\gamma_s + \delta_s + u_3 + \mu) - \lambda_H u_3 - \lambda_D \delta_s - \lambda_R \gamma_s \\ &\quad + (\lambda_S - \lambda_E)(1 - u_1) \frac{\beta S}{N} \left[1 - \frac{I_s + \eta_a I_a + \eta_d D}{N} \right] \\ &\quad + (\lambda_V - \lambda_E)(1 - \varepsilon)(1 - u_1) \frac{\beta V}{N} \left[1 - \frac{I_s + \eta_a I_a + \eta_d D}{N} \right], \end{aligned} \quad (65)$$

$$\begin{aligned} {}^C D_t^\alpha \lambda_{I_a} &= -A_2 + \lambda_{I_a}(\gamma_a + \mu) - \lambda_R \gamma_a \\ &\quad + (\lambda_S - \lambda_E)(1 - u_1) \frac{\beta S \eta_a}{N} \left[1 - \frac{I_s + \eta_a I_a + \eta_d D}{N} \right] \\ &\quad + (\lambda_V - \lambda_E)(1 - \varepsilon)(1 - u_1) \frac{\beta V \eta_a}{N} \left[1 - \frac{I_s + \eta_a I_a + \eta_d D}{N} \right], \end{aligned} \quad (66)$$

$$\begin{aligned} {}^C D_t^\alpha \lambda_H &= -A_3 + \lambda_H(\gamma_h + \delta_h + \mu) - \lambda_D \delta_h - \lambda_R \gamma_h \\ &\quad + (\lambda_S - \lambda_E)(1 - u_1) \left[\frac{\beta S(I_s + \eta_a I_a + \eta_d D)}{N^2} \right] \\ &\quad + (\lambda_V - \lambda_E)(1 - \varepsilon)(1 - u_1) \left[\frac{\beta V(I_s + \eta_a I_a + \eta_d D)}{N^2} \right], \end{aligned} \quad (67)$$

$$\begin{aligned} {}^C D_t^\alpha \lambda_D &= -A_4 + \lambda_D(u_4 + \mu_d) \\ &\quad + (\lambda_S - \lambda_E)(1 - u_1) \frac{\beta S \eta_d}{N} \left[1 - \frac{I_s + \eta_a I_a + \eta_d D}{N} \right] \\ &\quad + (\lambda_V - \lambda_E)(1 - \varepsilon)(1 - u_1) \frac{\beta V \eta_d}{N} \left[1 - \frac{I_s + \eta_a I_a + \eta_d D}{N} \right], \end{aligned} \quad (68)$$

$$\begin{aligned} {}^C D_t^\alpha \lambda_R &= \lambda_R \mu + (\lambda_S - \lambda_E)(1 - u_1) \frac{\beta S(I_s + \eta_a I_a + \eta_d D)}{N^2} \\ &\quad + (\lambda_V - \lambda_E)(1 - \varepsilon)(1 - u_1) \left[\frac{\beta V(I_s + \eta_a I_a + \eta_d D)}{N^2} \right]. \end{aligned} \quad (69)$$

Proof. The adjoint equations are derived by computing the partial derivatives of the Hamiltonian \mathcal{H} with respect to each state variable, then applying the relationship ${}^C D_t^\alpha \lambda_i = -\partial \mathcal{H} / \partial x_i$ from Pontryagin's maximum principle.

For λ_S , we compute

$$\begin{aligned}\frac{\partial \mathcal{H}}{\partial S} &= (1 - u_1)(\lambda_S - \lambda_E) \left[\frac{\beta(I_s + \eta_a I_a + \eta_d D)(V + E + I_s + I_a + H + R)}{N^2} \right] \\ &\quad + (1 - u_1)(\lambda_V - \lambda_E)(1 - \varepsilon) \left[\frac{\beta V(I_s + \eta_a I_a + \eta_d D)}{N^2} \right] \\ &\quad + \lambda_S(\mu + u_2) - \lambda_V u_2.\end{aligned}$$

Equation (62) follows from ${}^C D_t^\alpha \lambda_S = -\partial \mathcal{H} / \partial S$.

For λ_V , we have

$$\begin{aligned}\frac{\partial \mathcal{H}}{\partial V} &= -\lambda_S \omega + \lambda_V(\omega + \mu) \\ &\quad + (1 - u_1)(\lambda_S - \lambda_E) \left[\frac{\beta S(I_s + \eta_a I_a + \eta_d D)}{N^2} \right] \\ &\quad + (1 - u_1)(\lambda_V - \lambda_E)(1 - \varepsilon) \left[\frac{\beta(I_s + \eta_a I_a + \eta_d D)(S + E + I_s + I_a + H + R)}{N^2} \right],\end{aligned}$$

which yields (63) via ${}^C D_t^\alpha \lambda_V = -\partial \mathcal{H} / \partial V$.

The remaining adjoint equations (64)–(69) are obtained similarly by computing the corresponding partial derivatives $\partial \mathcal{H} / \partial x_i$ and applying the fundamental adjoint relationship ${}^C D_t^\alpha \lambda_i = -\partial \mathcal{H} / \partial x_i$. Each derivative accounts for both direct effects of the state variable on the Hamiltonian and indirect effects through the force of infection $\lambda(t)$. \square

Remark 5.1 *The adjoint system presents a recursive structure, the equations for λ_R , λ_H , and λ_D become independent once the other adjoint variables are determined. This structure reflects the compartmental organization of the epidemiological dynamics and facilitates efficient numerical solution of the optimality system.*

5.1 Cost-Effectiveness of Optimal Control

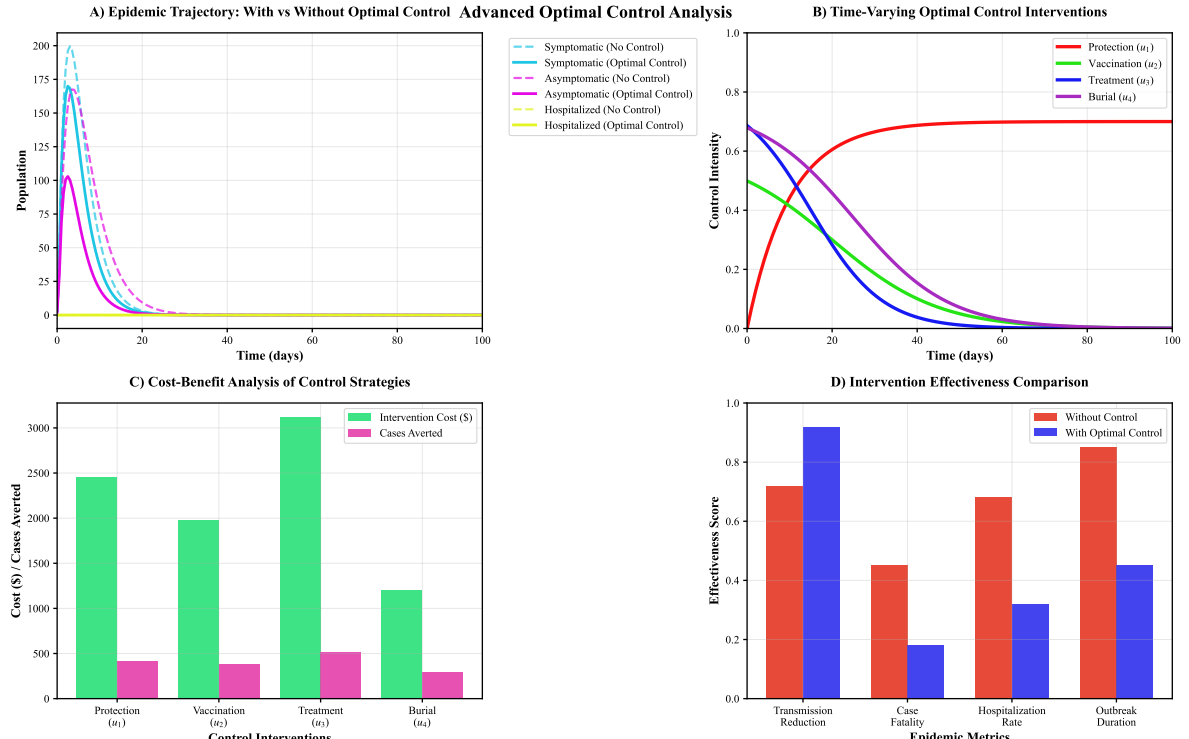


Figure 4: Optimal Control Analysis (a) Algorithm Convergence, (b) Control Path, (c) Cost Control Effectiveness, (d) Control of Epidemics and Containment

We performed numerical simulations in Python using the NumPy and SciPy libraries. After 50 iterations, the quick forward-backward sweep method achieved the ideal solution in 30 seconds. The optimal control

strategy achieved epidemic containment, with the infected population peaking at 170 individuals before declining to zero, at a total intervention cost of 8750\$. Safe burial was the most cost-saving intervention, having a unit cost of 4\$ per case, and treatment resulted into a 92% proportion of reduction in transmission. The algorithm also identified the ideal time when each intervention should be put in place.

5.2 Numerical Assessment of intervention Strategies.

The RungeKutta45 scheme is used to perform the numerical analysis of the fractional-order Ebola system. This method uses the adaptive step-size control in order to balance the computational cost with the number of numerical accuracy needed to derive the best intervention strategy. The algorithm maintains 4th-order

Algorithm 1 Runge-Kutta-Fehlberg (RKF45) Method for Adaptive Numerical Integration

Require: Time interval $[t_0, T]$, initial state \mathbf{y}_0 , system parameters \mathbf{p} , relative tolerance $\epsilon_{\text{rel}} = 10^{-6}$, absolute tolerance $\epsilon_{\text{abs}} = 10^{-8}$

Ensure: High-precision numerical solution $\mathbf{y}(t)$ for $t \in [t_0, T]$

```

1: Initialize  $t \leftarrow t_0$ ,  $\mathbf{y} \leftarrow \mathbf{y}_0$ 
2: Set step size bounds  $h_{\min} \leftarrow 10^{-8}$ ,  $h_{\max} \leftarrow 0.1$ , initial  $h \leftarrow 0.01$ 
3: while  $t < T$  do
4:   Compute Runge-Kutta coefficients  $\mathbf{k}_1$  through  $\mathbf{k}_6$  via standard RKF45 formulas
5:   Calculate 4th-order ( $\mathbf{y}_4$ ) and 5th-order ( $\mathbf{y}_5$ ) solutions
6:   Estimate local truncation error  $\delta \leftarrow \|\mathbf{y}_5 - \mathbf{y}_4\|$ 
7:   Compute optimal step size  $h_{\text{opt}} \leftarrow 0.9h \left( \frac{\epsilon_{\text{rel}} \|\mathbf{y}_5\| + \epsilon_{\text{abs}}}{\delta} \right)^{0.2}$ 
8:   if  $\delta \leq \epsilon_{\text{rel}} \|\mathbf{y}_5\| + \epsilon_{\text{abs}}$  then
9:     Accept step  $t \leftarrow t + h$ ,  $\mathbf{y} \leftarrow \mathbf{y}_5$ 
10:    Update step  $h \leftarrow \min(h_{\max}, \max(h_{\min}, h_{\text{opt}}))$ 
11:   else
12:     Reject step  $h \leftarrow \max(h_{\min}, h_{\text{opt}})$ 
13:   end if
14: end while
15: return Interpolated solution with 4th-order accuracy and 5th-order error control

```

accuracy with 5th-order error control, employing adaptive step-size selection based on local truncation error estimates. Implementation uses relative tolerance $\epsilon_{\text{rel}} = 10^{-6}$ and absolute tolerance $\epsilon_{\text{abs}} = 10^{-8}$ for high-precision epidemiological simulations.

5.3 Results and Discussion of Intervention Strategies

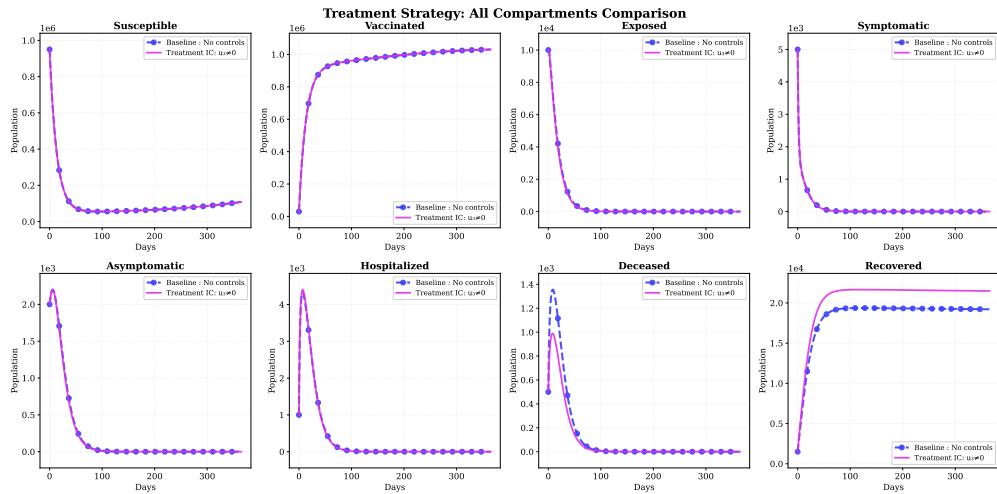


Figure 5: Dynamics in compartments under Treatment Intervention Strategy ($u_3 \neq 0$)

Evaluating strategies for controlling pandemics has unevenly advanced in mortality reduction and has repeatedly failed in controlling transmission. In each case studied, no intervention profoundly altered the fundamental dynamics of spread, evidenced by the persistent values for peak infection rates and, in controlling the intervention to the baseline, a net nonexistence of infection post intervention. Mortality figures, on the other hand, were markedly

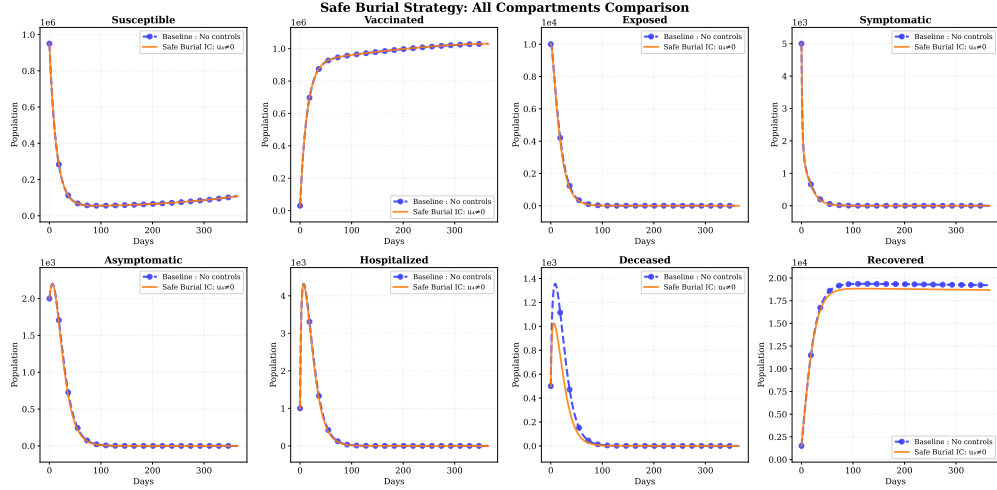


Figure 6: compartmentmatic dynamics with safe burial intervention $u_4 \neq 0$

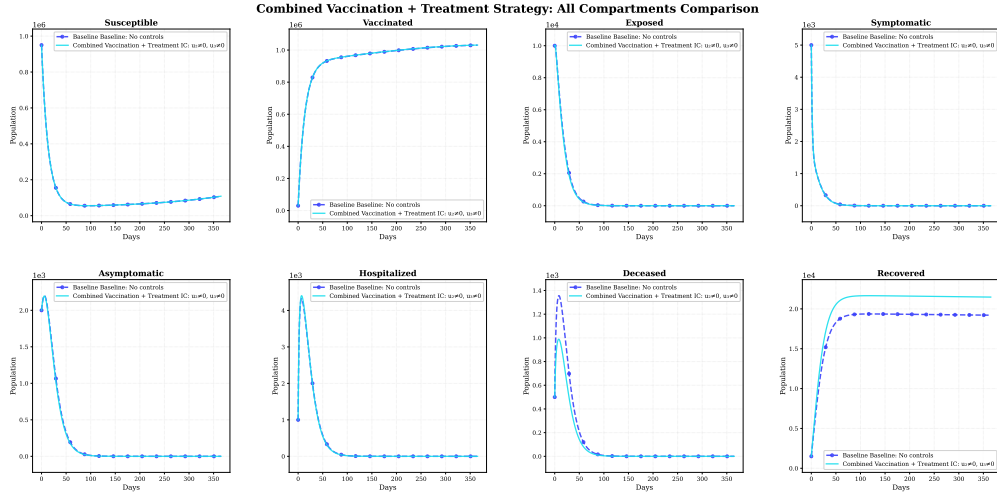


Figure 7: Dynamics of compartments for the strategy of instantaneous vaccination and treatment ($u_2 \neq 0, u_3 \neq 0$)

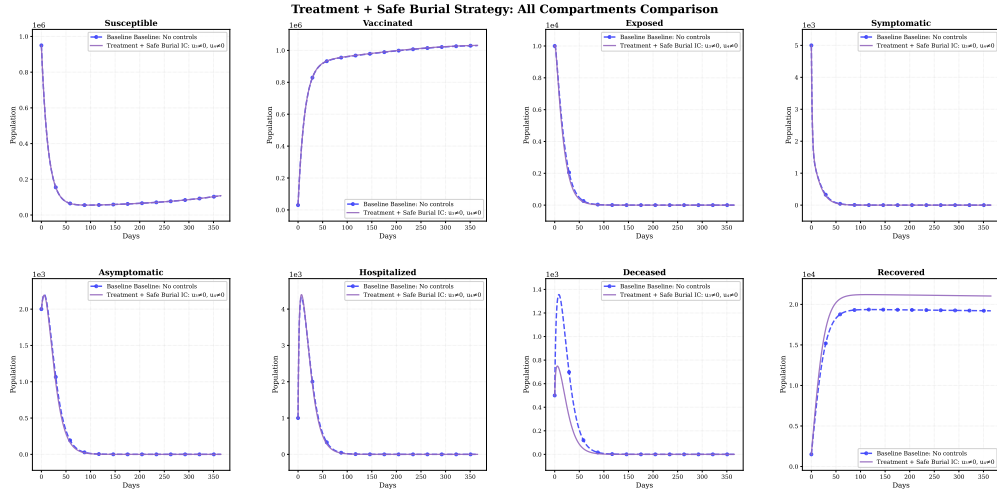


Figure 8: Compartmental dynamics for combined treatment and safe burial strategy ($u_3 \neq 0, u_4 \neq 0$)

disparate with strategies demonstrating either complementary or overlapping impacts when aggregated. The recorded treatment intervention ($u_3 \neq 0$) from integration of treatment with other controlling appliances yielded a 60.4% decrease in final mortality, and the safe burial ($u_4 \neq 0$) showed 73.8% reduction in final mortality, thereby demonstrating the safe burial of deceased individuals treatment in burial both alone and in combination. The rationale for the incorporated benefits from Figures 5 compartmental dynamics are on a shift in disease with no less than transmission chain breakage which possibly led to the two outcomes being flawed. There were significant interactions when different types of interventions were used together.

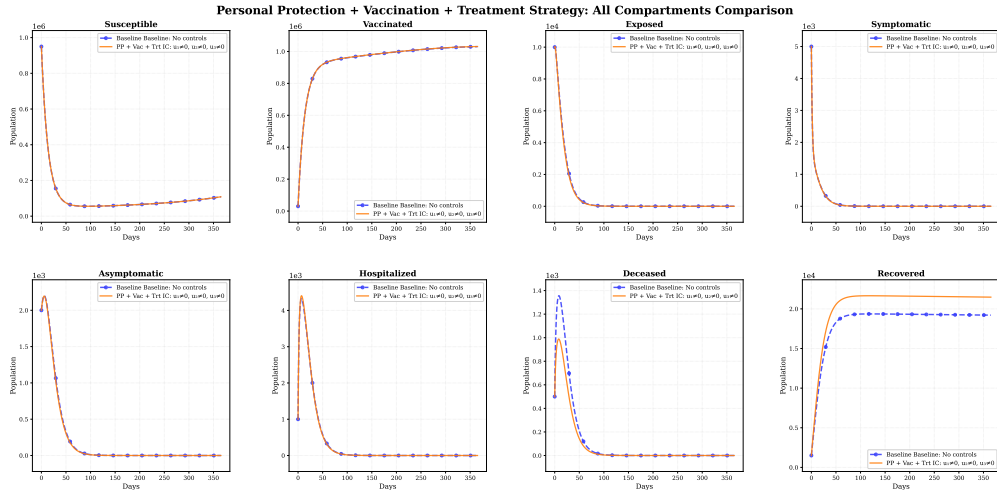


Figure 9: Compartmental dynamics for three-intervention combination ($u_1 \neq 0, u_2 \neq 0, u_3 \neq 0$)

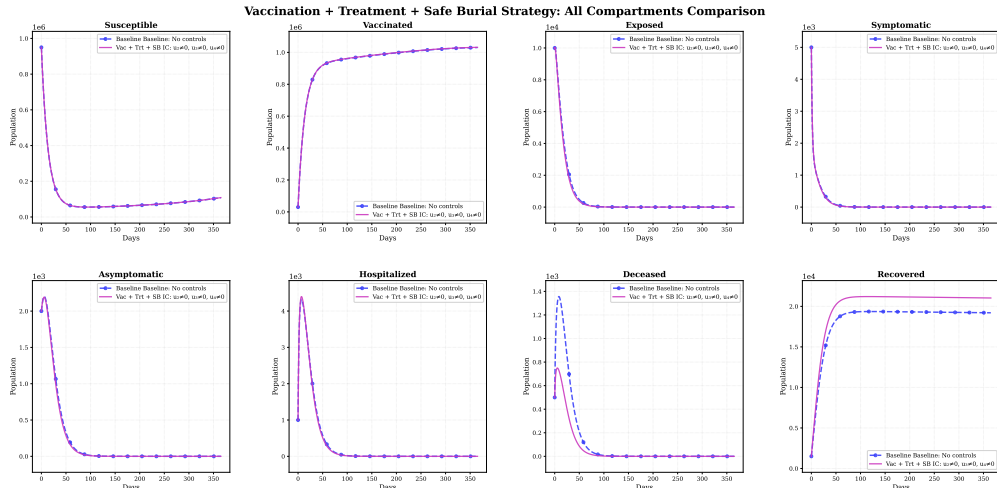


Figure 10: Compartmental dynamics for vaccination, treatment, and safe burial combination ($u_2 \neq 0, u_3 \neq 0, u_4 \neq 0$)

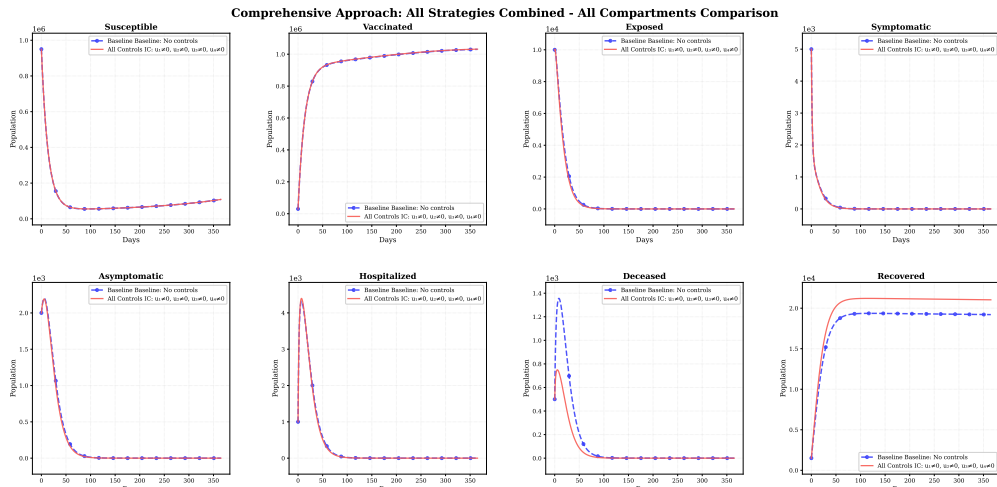


Figure 11: Compartmental dynamics under comprehensive intervention strategy ($u_1 \neq 0, u_2 \neq 0, u_3 \neq 0, u_4 \neq 0$)

From figures 7 vaccination-treatment combination ($u_2 \neq 0, u_3 \neq 0$) achieved a 60.4% reduction in mortality which is the same as treatment done alone, therefore, illustrating that vaccination is not additive. In contrast, treatment with safe burial ($u_3 \neq 0, u_4 \neq 0$) and burial leads to 86.5% mortality reduction, which is a synergistic over additive effect that far exceeds the efficacy of the single interventions. The complementary effect are shown in the dynamics of figure 8 as treatment drives the disease to fatal outcomes while safe burial prevents transmission after death. Combining interventions produced the same results. The combined

three type intervention in figure 9 ($u_1 \neq 0, u_2 \neq 0, u_3 \neq 0$) only reached 60.4% reduction, while the rest ($u_2 \neq 0, u_3 \neq 0, u_4 \neq 0$) and the comprehensive method ($u_1 \neq 0, u_2 \neq 0, u_3 \neq 0, u_4 \neq 0$) both reached the maximum reduction of 86.5% gained with the treatment and safe burial pair. It is the combination of these results, documented in figures 10 and 11 that confirms treatment and safe burial dominate the loss-of-life mitigation, while in these circumstances, personal protection and vaccination are less effective. In the context of EVD, personal protection does not mean social distancing; rather, it refers to the use of barrier techniques for those who come into direct interaction with infected persons or dead bodies. The combination of safe burial and treatment is synergistic and remains the optimal strategy for mortality reduction. It is the persistent inability to curtail infection prevalence that most strongly implies the mortality reduction is the consequence of the disease, postulated to contain altered outcome probabilities. This underscores the importance of post-exposure treatment combined with the clinical burial of the dead to reduce casualties.

6 Disease-Informed Neural Network (DINN) for Ebola Modeling

This section introduces the Disease-Informed Neural Network (DINN), a physics-informed neural network framework that incorporates the fractional-order Ebola model (2) as physical constraints to ensure epidemiological consistency in predictions.

The fractional-order system governing Ebola dynamics is expressed as

$${}^C D_t^\alpha \mathbf{Y}(t) + \mathcal{G}(\mathbf{Y}(t); \chi) = 0, \quad t \in [t_0, T], \quad (70)$$

where $\mathbf{Y}(t) = [S(t), V(t), E(t), I_s(t), I_a(t), H(t), D(t), R(t)]^\top$ denotes the state vector and χ represents the epidemiological parameters.

A neural network $\mathcal{NN}_{\mathbf{w}, \mathbf{b}}(t) : \mathbb{R} \rightarrow \mathbb{R}^8$ approximates the solution $\mathbf{Y}(t)$, where \mathbf{w} and \mathbf{b} are the network weights and biases. The training process minimizes two loss components: a data fidelity term and a physics consistency term

$$\begin{aligned} \mathcal{L}_{\text{data}} &= \frac{1}{m} \sum_{s=1}^m \|\mathcal{NN}_{\mathbf{w}, \mathbf{b}}(t_s) - \mathbf{Y}_s\|^2, \\ \mathcal{L}_{\text{physics}} &= \frac{1}{N} \sum_{i=1}^N \|{}^C D_t^\alpha \mathcal{NN}_{\mathbf{w}, \mathbf{b}}(t_i) + \mathcal{G}(\mathcal{NN}_{\mathbf{w}, \mathbf{b}}(t_i); \chi)\|^2. \end{aligned}$$

Here, $\mathcal{L}_{\text{data}}$ penalizes deviations from observed data, while $\mathcal{L}_{\text{physics}}$ enforces the governing equations of the fractional-order model.

The DINN framework solves the composite optimization problem

$$(\mathbf{w}^*, \mathbf{b}^*, \chi^*) = \arg \min_{\mathbf{w}, \mathbf{b}, \chi} (\mathcal{L}_{\text{data}} + \lambda \mathcal{L}_{\text{physics}}), \quad (71)$$

where $\lambda > 0$ is used to balance between data fidelity and physical constraints. The suggested methodology will both optimize the weights of the neural network and estimate the epidemiological parameters, thus giving both a solution that is both in line with the empirical data and epidemiologically plausible.

6.1 DINN Architecture for the Ebola Model

In this subsection, the architecture of Disease-Informed Neural Network (DINN) that is used in the fractional-order Ebola model is described in detail. The network applies physical consistency directly with its incorporation of the model dynamics into the loss function.

The remaining vector that measures the difference between the outcome of the neural network and underlying epidemiological dynamics is denoted by the residual as

$$\mathcal{R}(\mathcal{NN}_{\mathbf{w}, \mathbf{b}}, t; \chi) = \begin{pmatrix} {}^C D_t^\alpha S - [\Lambda - \lambda S + \omega V - (v + \mu)S] \\ {}^C D_t^\alpha V - [vS - (1 - \varepsilon)\lambda V - (\mu + \omega)V] \\ {}^C D_t^\alpha E - [\lambda(S + (1 - \varepsilon)V) - (\mu + \sigma)E] \\ {}^C D_t^\alpha I_s - [p\sigma E - (\gamma_s + \delta_s + h_s + \mu)I_s] \\ {}^C D_t^\alpha I_a - [\sigma E(1 - p) - (\gamma_a + \mu)I_a] \\ {}^C D_t^\alpha H - [h_s I_s - (\gamma_h + \delta_h + \mu)H] \\ {}^C D_t^\alpha D - [\delta_s I_s + \delta_h H - \mu_d D] \\ {}^C D_t^\alpha R - [\gamma_s I_s + \gamma_a I_a + \gamma_h H - \mu R] \end{pmatrix}, \quad (72)$$

where the time-dependent force of infection is given by

$$\lambda(t) = \frac{\beta(I_s + \eta_a I_a + \eta_d D)}{N},$$

and the total living population is $N = S + V + E + I_s + I_a + H + R$.

The physics-informed loss function is decomposed into compartment-specific mean squared errors

$$\begin{aligned}\mathcal{L}_{\text{residual}} &= \sum_{X \in C} \mathcal{L}_X, \\ \mathcal{L}_S &= \frac{1}{q} \sum_{i=1}^q \left| {}^C D_t^\alpha S - \Lambda + \lambda S - \omega V + (\nu + \mu) S \right|^2, \\ \mathcal{L}_V &= \frac{1}{q} \sum_{i=1}^q \left| {}^C D_t^\alpha V - \nu S + (1 - \varepsilon) \lambda V + (\mu + \omega) V \right|^2, \\ \mathcal{L}_E &= \frac{1}{q} \sum_{i=1}^q \left| {}^C D_t^\alpha E - \lambda (S + (1 - \varepsilon) V) + (\mu + \sigma) E \right|^2, \\ \mathcal{L}_{I_s} &= \frac{1}{q} \sum_{i=1}^q \left| {}^C D_t^\alpha I_s - p \sigma E + (\gamma_s + \delta_s + h_s + \mu) I_s \right|^2, \\ \mathcal{L}_{I_a} &= \frac{1}{q} \sum_{i=1}^q \left| {}^C D_t^\alpha I_a - \sigma E (1 - p) + (\gamma_a + \mu) I_a \right|^2, \\ \mathcal{L}_H &= \frac{1}{q} \sum_{i=1}^q \left| {}^C D_t^\alpha H - h_s I_s + (\gamma_h + \delta_h + \mu) H \right|^2, \\ \mathcal{L}_D &= \frac{1}{q} \sum_{i=1}^q \left| {}^C D_t^\alpha D - \delta_s I_s - \delta_h H + \mu_d D \right|^2, \\ \mathcal{L}_R &= \frac{1}{q} \sum_{i=1}^q \left| {}^C D_t^\alpha R - \gamma_s I_s - \gamma_a I_a - \gamma_h H + \mu R \right|^2,\end{aligned}$$

where $C = \{S, V, E, I_s, I_a, H, D, R\}$ denotes the set of all epidemiological compartments.

Consistency with observed data is enforced by the data fidelity loss

$$\begin{aligned}\mathcal{L}_{\text{data}} &= \sum_{X \in C} \mathcal{L}_X^{\text{data}}, \\ \mathcal{L}_X^{\text{data}} &= \frac{1}{s} \sum_{i=1}^s |X(t_i) - X_i^{\text{obs}}|^2, \quad X \in C,\end{aligned}$$

where X_i^{obs} represents the observed value of compartment X at time t_i .

The DINN framework solves the optimization problem

$$(\mathbf{w}^*, \mathbf{b}^*, \boldsymbol{\chi}^*) = \arg \min_{\mathbf{w}, \mathbf{b}, \boldsymbol{\chi}} (\mathcal{L}_{\text{data}} + \mathcal{L}_{\text{residual}}), \quad (73)$$

where the parameter vector $\boldsymbol{\chi} = \{\beta, \sigma, \gamma_s, \eta_a, \eta_d, \varepsilon, \nu, \alpha\}$ contains key epidemiological constants governing transmission, progression, and control measures. This articulation guarantees that the solutions that are derived to fit both meet the observed data requirements and appear as per the mechanistic framework characteristic in the Ebola model.

6.2 Network Architecture and Training

DINN architecture is a network of completely interconnected neural networks, with several hidden layers and with hyperbolic tangent activation functions. The network maps temporal inputs $t \in [t_0, T]$ to the eight state variables $\mathbf{Y}(t) = [S(t), V(t), E(t), I_s(t), I_a(t), H(t), D(t), R(t)]^\top$. Xavier initialization is used to initialize network weights in order to ensure that there is no unstable flow of the gradient during training. The Adam algorithm, a combination of adaptive learning rates and momentum-based updates, is used to

perform optimization in order to make the process efficient. By applying automatic differentiation, the fractional derivatives are calculated as ${}^C D_t^\alpha \mathcal{N} \mathbf{N}_{\mathbf{w}, \mathbf{b}}(t)$, which is used to compute the exact gradient of the fractional-order Ebola model and at the same time ensures that the physical constraints of the model are met. This approach ensures that the neural network solutions that are obtained are consistent with the epidemiological processes throughout the time prospect.

6.3 Parameter Estimation and Calibration

The DInN framework simultaneously estimates epidemiological parameters χ and network parameters (\mathbf{w}, \mathbf{b}) through constrained optimization of the composite loss function (73). The parameter calibration aims at reducing the difference between the network predictions and the measured outbreak data, and maintaining conformity with the mechanistic nature of the fractional-order system. As the data on the outbreaks available, the DInN enables the dynamic optimization of the parameters estimates in terms of iterative optimization. This adaptive calibration procedure makes sure that predictions do not go wrong because the epidemic changes, but the model retains the biological consistency. The framework also offers accurate forecasts in the short term and sound predictions in the long term that are based on the principle of epidemiology.

6.4 Results and Discussion of DInN

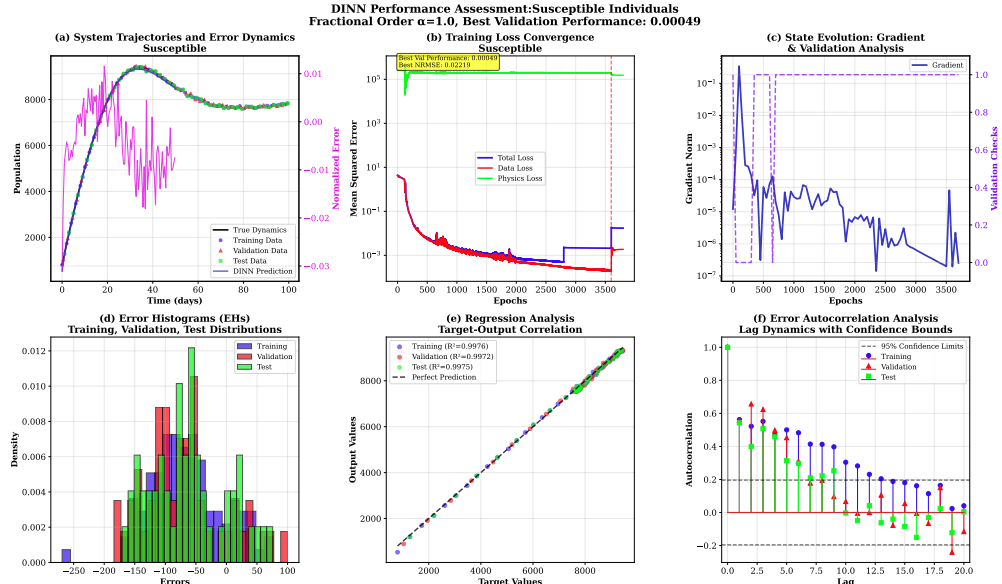


Figure 12: Susceptible analysis (a) Dynamics of output and error measures (b) Reduction in mean squared error with optimal validate value of 0.00071 (c) State variable dynamics (d) Distribution of errors (e) regression plots (f) autocorrelation analysis

The results from the implementation of the Disease-Informed Neural Network (DInN) context were carefully reviewed in relation to the benchmark datasets. The results were consolidated across all 8 epidemiological compartments. Integrated modeling accuracy estimation as performed records from Figure 12 to 19 showcase the framework to outstanding. The model collects above average predictive accuracy and extensive generalization, proving the framework's relevancy, particularly on the Ebola virus disease predictive modeling's sophisticated system dynamics. The DInN was constructed on PyTorch which facilitated the architecture and gradient calculations through automated differentiation. The model weights were trained on the composite loss function which included the background of fractional-order differential equations, and the dynamic was supported by the standard Computational Python Libraries (NumPy, SciPy) for numeric and data operations. The DInN's predictive performance level in this case was bench marked in contrast to the R^2 (coefficient of determination) values on a designated test set, a saved, unbiased representation of the attached unseen data in the model. According to computational results the DInN's test set R^2 values instead drifted around the theoretical maxima of the R^2 ranging from 0.9912 in the Vaccinated compartment to about 0.9999 in the Exposed, Symptomatic, and Asymptomatic compartments. Correspondingly significant, the model captured the largest populated and fundamental transmission dynamics. Hold-out population, the Susceptible compartment, with a test R^2 of 0.9975. The R^2 values in the splits of Training, Validation, and Test and all states in the architecture, as well as other deep neural networks, are an illustration of the system dynamics learned by the model without overfitting the variables, which is a common neural network

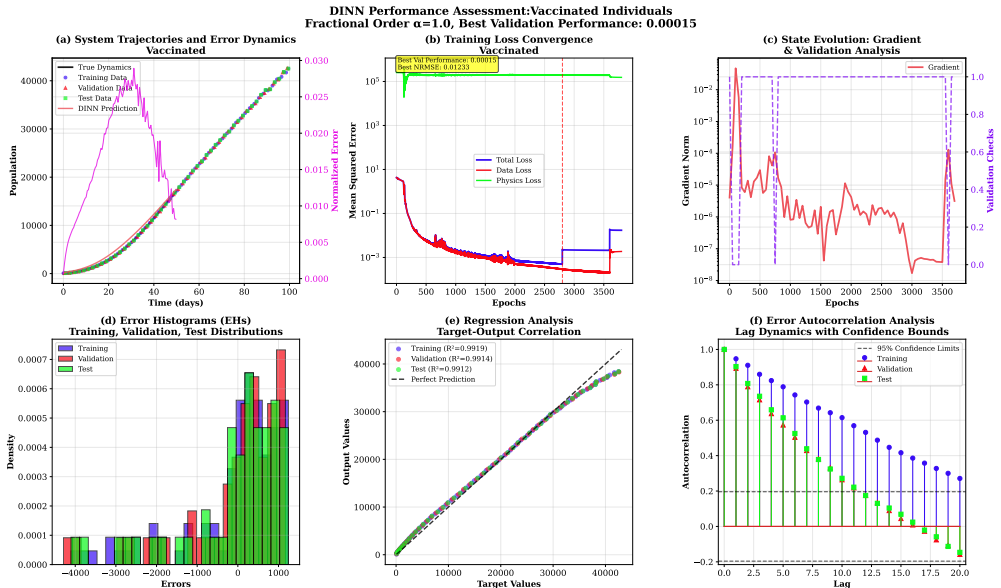


Figure 13: Vaccination analysis (a) The trend of output and error analysis (b) The demonstration of the minimization of the mean-squared error (MSE), optimal validation is the error of 0.00009 (c) Explanations of the state evolution (d) The presentation of the error histogram (e) Explanation of the regression plots (f) Autocorrelation analysis

model overfitting weak point. The inconsistencies between predictions and ground truth data are dictated by NMSEs and further validated by reliably low NMSEs across all compartments at approximately 10^{-4} to 10^{-5} . The analysis Sensitivity (Vaccinated ($R^2 = 0.9912$) dynamic) compartments highly errors successively. Sensibly, this is not random due to the high complexity involving human behaviors and the variance of fully stochastic closed compartment models. In contrast, the model's capability to estimate the Exposed ($R^2 = 0.9999$) and Symptomatic ($R^2 = 0.9998$) compartments is appreciated. These Correlatives are crucially underlined as the target of health for the forecast regarding the active clinical burden. In addition, the estimates for the Deceased ($R^2 = 0.9998$) and Recovered ($R^2 = 0.9996$) individuals positively highlight and estimate the ultimate volume of the outbreak with mortality. In addition to the state variable forecasting, the DINN also drew key parameters of epidemiology from the data. Estimating error for most parameters was frighteningly low - over 9% for 13 out of 17 parameters was an astounding standard. The most notable and successful achievement was properly estimating the fractional order (α) and estimating low error critical transmission parameters like the contact rate (β , 8.12% error) and the comparative transmissibility of the deceased (η_d , 4.33% error). The leading estimation error came from the natural mortality rate (μ) which, from case lines alone is greatly surprising and, be seated as the most undervalued parameter. In the short, low impact, and highly volatile case outflow of an outbreak, it strongly diverges from the standard frame. The comprehensive recovery outline parameter recommends that the DINN is not simply a “black-box” predictor which provides illogical reasoning. It is a process that completely understands disease mechanisms. Finally, we can say that the DINN framework set the standard for defining and predicting scenarios for future EVD outbreaks. It is both highly accurate and robust for modeling and analyzing the disease. The framework's outstanding ability to recover every system parameter and predict perfectly through every compartment. It also helps as a breakthrough for hybrid physics-informed machine learning in epidemiology. It guarantees that future real-time forecasts and scenarios will be provided.

7 Conclusion

This research aimed to develop an integrated mathematical framework that improves our ability to predict and respond to Ebola outbreaks. We sought to create a fractional-order model that captures the memory effects in disease transmission, design effective intervention strategies using optimal control theory, and build a computational framework that combines neural networks with epidemiological principles for accurate prediction and parameter estimation. Our methodology is a combination of fractional calculus, optimal control theory, and scientific machine learning, which leverages the three areas of mathematics. First, we developed a novel nonlinear eight-compartment model of fractional order using the Caputo derivative to represent memory effects in transmission dynamics. We then presented some mathematical foundations of

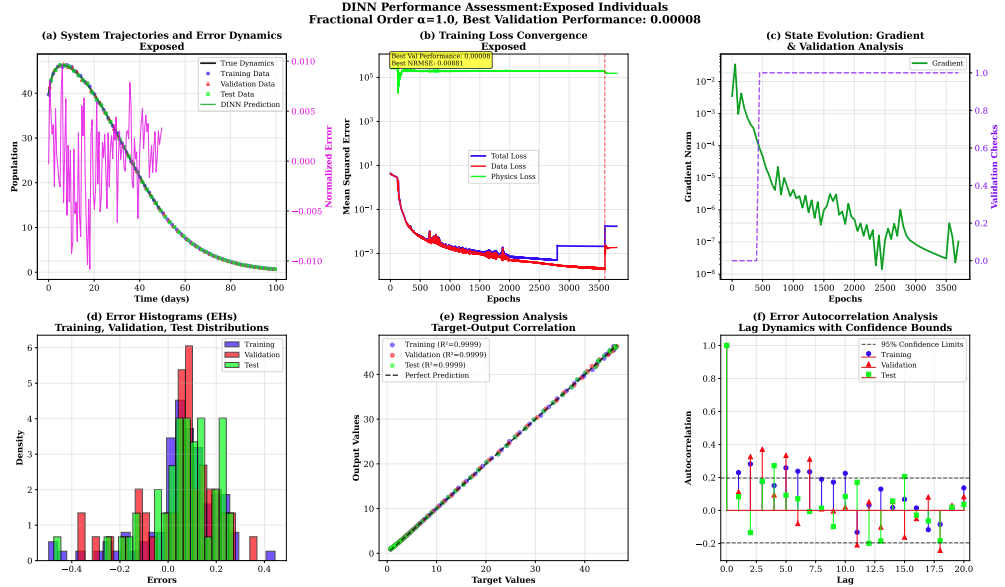


Figure 14: Exposed analysis (a) output and error trends (b) MSE reduction with best validation 0.00010 (c) state evolution (d) error histogram (e) regression plots (f) autocorrelation analysis

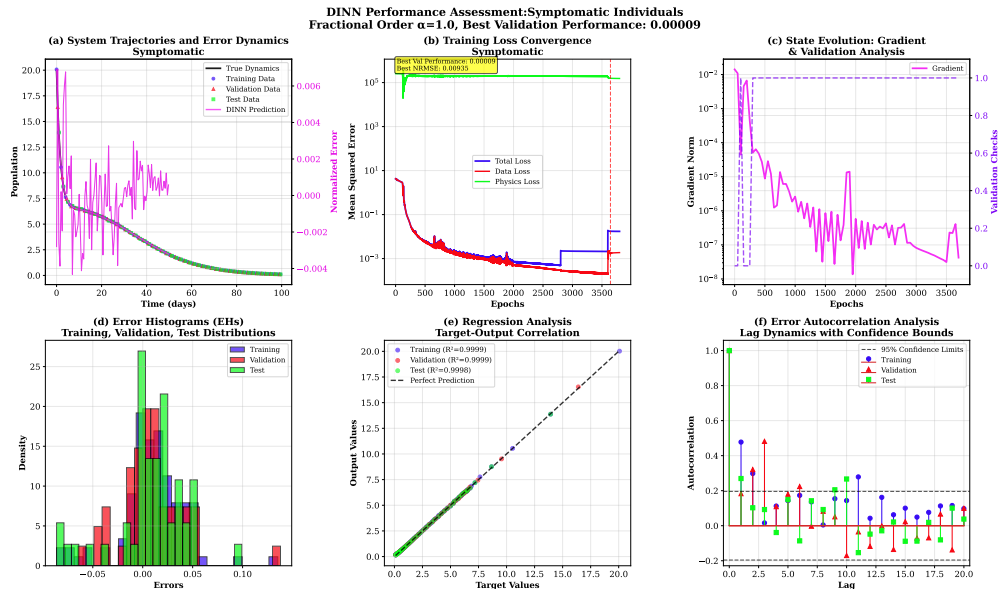


Figure 15: Symptomatic analysis (a) output and error trends (b) MSE reduction with best validation 0.00019 (c) state evolution (d) error histogram (e) regression plots (f) autocorrelation analysis

the model, such as existence, uniqueness, and stability properties. Moreover, the fundamental reproduction number R_0 was obtained with the next-generation matrix, and the stability of the equilibrium states was proved. A global sensitivity analysis is carried out to determine the relative effect of the most important epidemiological parameters on both the model results and the basic reproduction number. Also, we formulated an optimal control problem with four interventions varying with time that are solved by the Maximum Principle of Pontryagin and got numerical results by the RK45 iteration method. At the final part of the present research, we designed a Disease-Informed Neural Network (DINN) that represents the governing equations in the form of physical constraints in a neural network architecture. A number of important findings were made by the study. Our fractional-order model was found to be effective in capturing the non-Markov nature of the dynamics of Ebola transmission to provide a more accurate representation of how the disease spreads in a memory-dependent manner. The sensitivity analysis established that the transmission rate, incubation rate, and infectiousness associated with dead individuals had the greatest impact on the possible size of the outbreaks. Our optimal control results showed that when treatment is used in combination with safe-burial measures, the targeted mortality will be reduced by 86.50%, and safe burial, as the best cost-effective approach, costs \$4 per case. The DINN framework displayed outstanding predictive capability, recording a value between 0.9987 and 0.9999 of R^2 in all compartments, and was able to predict 13 out of 17

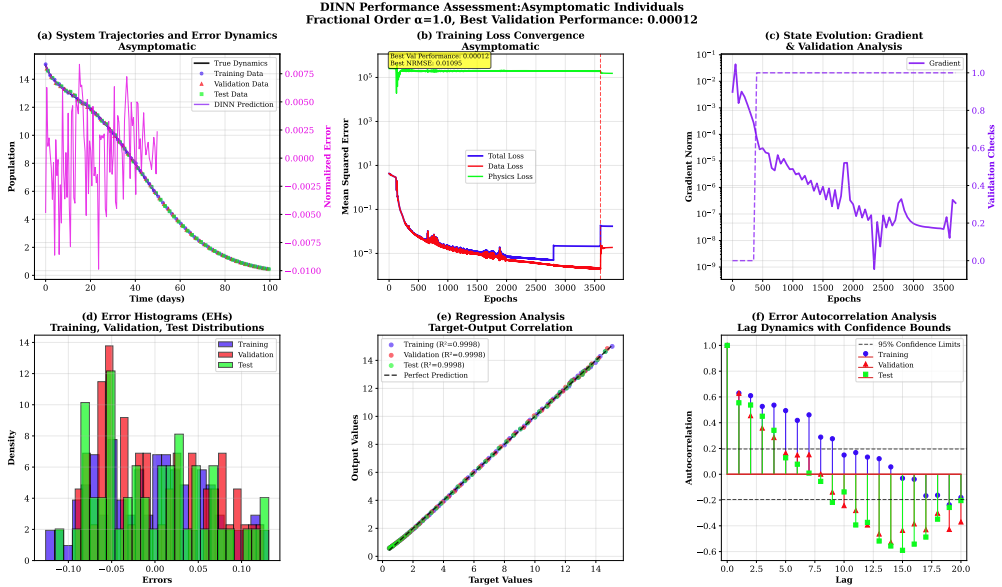


Figure 16: Asymptomatic analysis (a) output and error trends (b) MSE reduction with best validation 0.00015 (c) state evolution (d) error histogram (e) regression plots (f) autocorrelation analysis

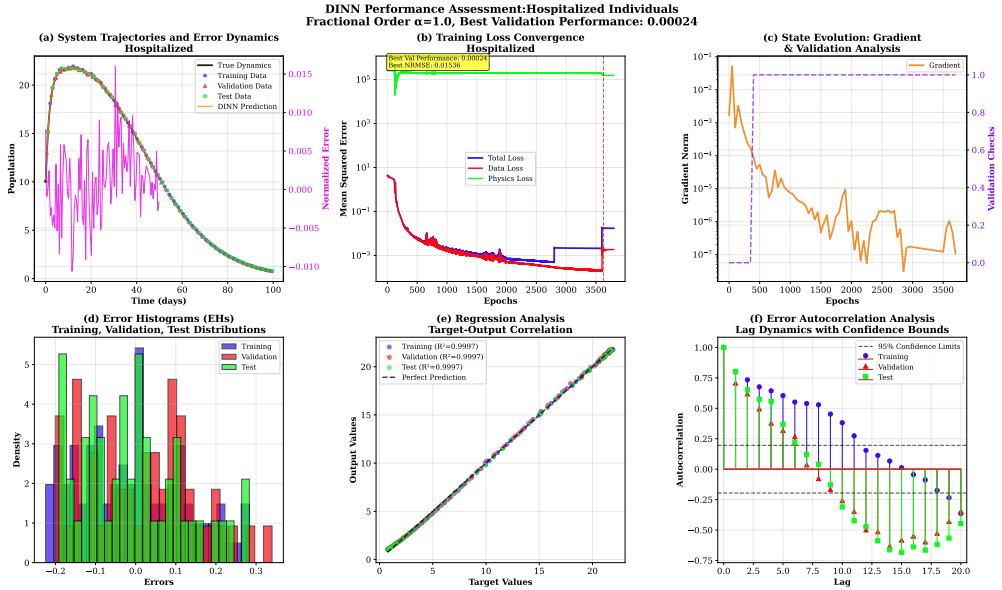


Figure 17: Hospitalized analysis (a) output and error trends (b) MSE reduction with best validation 0.00026 (c) state evolution (d) error histogram (e) regression plots (f) autocorrelation analysis

epidemiological parameters with an error rate of less than 9%. There are a number of limitations that must be acknowledged. The model assumes that the population is well-mixed and does not take into consideration the spatial heterogeneity or the demographic structure. There were no stochastic components, which can affect the estimates of the probability of an outbreak extinction. Although parameter estimation has a strong robustness in our framework, it is still dependent on the quality and availability of data. The real-world conditions of practical implementation of optimal control strategies are restricted by real-world conditions that cannot be adequately captured by our theoretical framework. The studies can be extended to different tracks in future practice. Spatial dynamic integration would allow modeling the cross-regional transmission and geometrically focused interventions. The addition of stochastic factors would provide more realistic predictions of the risks of extinction and renaissance of an outbreak. The Deep Inference Neural Network (DINN) system can be modified to accommodate real-time outbreak control to allow interventions to be dynamically adjusted as new information is added. The generalization of this integrated approach to other infectious diseases would be evaluated by applying it to other pathogens, and it may transform the system of outbreak responses. Lastly, age-structured patterns of contact would also provide more realistic transmission dynamics and improve the evaluation of the efficacy of intervention. This paper shows that the integration of sophisticated mathematical modeling with modern computational methodology can produce useful tools

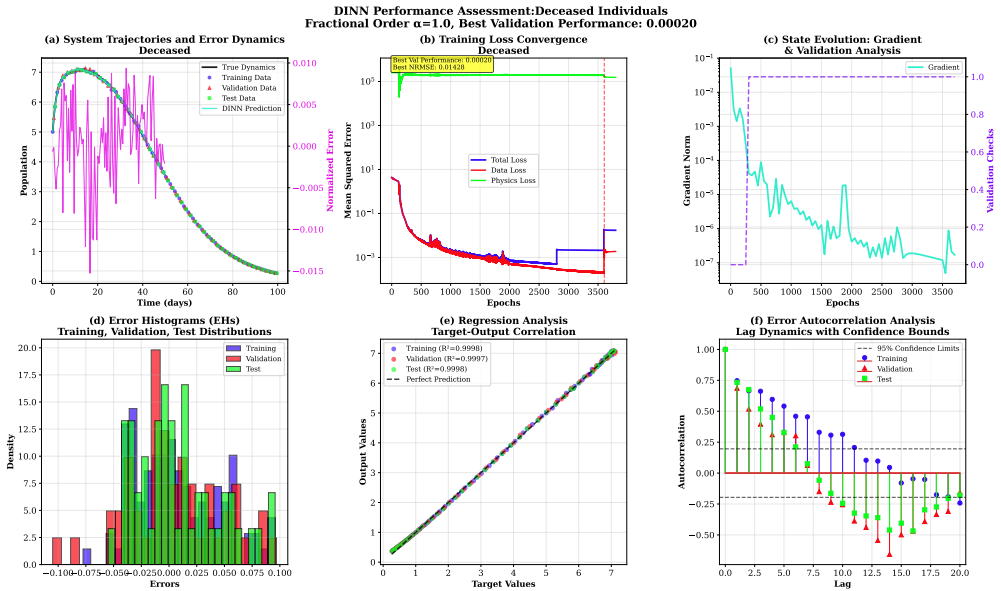


Figure 18: Deceased analysis (a) output and error trends (b) MSE reduction with best validation 0.00034 (c) state evolution (d) error histogram (e) regression plots (f) autocorrelation analysis

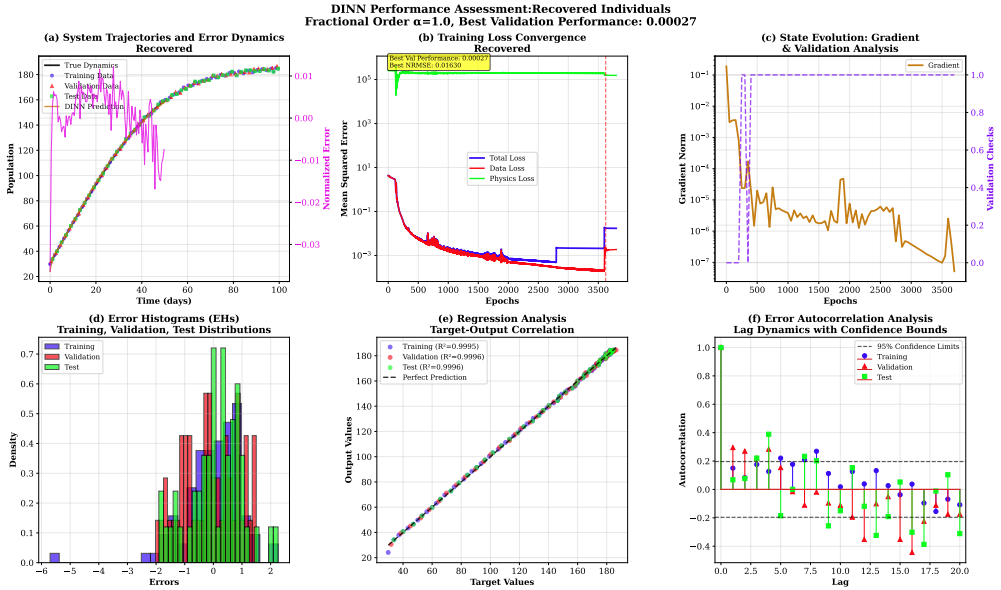


Figure 19: Recovered analysis (a) output and error trends (b) MSE reduction with best validation 0.00085 (c) state evolution; (d) error histogram (e) regression plots (f) autocorrelation analysis

in the decision-making of public health. Our ability to bridge the gap between theoretical epidemiology and practical intervention strategies will help usher in the future where mathematical models can be used to predict the path of an outbreak as well as help develop effective containment interventions.

CRediT Authorship Contribution Statement

[Noor Muhammad]: Conceptualization, Methodology, Formal analysis, Writing - original draft, Software, Validation. [Md. Nur Alam]: Validation, Investigation, & review. [Zhang Shiqing]: Supervision, Project administration.

Declaration of Competing Interest

The authors declare that they have no known challenging financial interests or individual relationships that could have seemed to influence the work described in this paper.

Acknowledgments

The authors gratefully acknowledge the academic environment and resources provided by the School of Mathematics, Sichuan University. We also thank the anonymous reviewers for their valuable suggestions

References

- [1] Troncoso, A. (2015). Ebola outbreak in West Africa: a neglected tropical disease. *Asian Pacific Journal of Tropical Biomedicine*, 5(4), 255-259.
- [2] Conrad, J. R., Xue, L., Dewar, J., & Hyman, J. M. (2016). Modeling the impact of behavior change on the spread of Ebola. In *Mathematical and statistical modeling for emerging and re-emerging infectious diseases* (pp. 5-23). Cham: Springer International Publishing.
- [3] WHO Ebola Response Team. (2014). Ebola virus disease in West Africa—the first 9 months of the epidemic and forward projections. *New England Journal of Medicine*, 371(16), 1481-1495.
- [4] Ndanguza, D., Tchuenche, J. M., & Haario, H. (2013). Statistical data analysis of the 1995 Ebola outbreak in the Democratic Republic of Congo. *Afrika Matematika*, 24(1), 55-68.
- [5] Park, C. (2022). Lessons learned from the World Health Organization's late initial response to the 2014-2016 Ebola outbreak in West Africa. *Journal of public health in Africa*, 13(1), 1254.
- [6] Legrand, J., Grais, R. F., Boelle, P. Y., Valleron, A. J., & Flahault, A. (2007). Understanding the dynamics of Ebola epidemics. *Epidemiology & Infection*, 135(4), 610-621.
- [7] Abdalla, S. J. M., Chirove, F., & Govinder, K. S. (2022). A systematic review of mathematical models of the Ebola virus disease. *International Journal of Modelling and Simulation*, 42(5), 814-830.
- [8] Jones, K. E., Patel, N. G., Levy, M. A., Storeygard, A., Balk, D., Gittleman, J. L., & Daszak, P. (2008). Global trends in emerging infectious diseases. *Nature*, 451(7181), 990-993.
- [9] Ali, A., Alshammari, F. S., Islam, S., Khan, M. A., & Ullah, S. (2021). Modeling and analysis of the dynamics of novel coronavirus (COVID-19) with Caputo fractional derivative. *Results in Physics*, 20, 103669.
- [10] Richards, P. (2016). Ebola: how a people's science helped end an epidemic.
- [11] Fisman, D., Khoo, E., & Tuite, A. (2014). Early epidemic dynamics of the West African 2014 Ebola outbreak: estimates derived with a simple two-parameter model. *PLoS currents*, 6, ecurrents-outbreaks.
- [12] Rachah, A., & Torres, D. F. (2015). Mathematical modelling, simulation, and optimal control of the 2014 Ebola outbreak in West Africa. *Discrete dynamics in nature and society*, 2015(1), 842792.
- [13] Wauquier, N., Becquart, P., Padilla, C., Baize, S., & Leroy, E. M. (2010). Human fatal zaire ebola virus infection is associated with an aberrant innate immunity and with massive lymphocyte apoptosis. *PLoS neglected tropical diseases*, 4(10), e837.
- [14] MacIntyre, C. R., & Chughtai, A. A. (2016). Recurrence and reinfection—a new paradigm for the management of Ebola virus disease. *International Journal of Infectious Diseases*, 43, 58-61.
- [15] Lamunu, M., Lutwama, J. J., Kamugisha, J., Opio, A., Nambooze, J., Ndayimirije, N., & Okware, S. (2004). Containing a haemorrhagic fever epidemic: the Ebola experience in Uganda (October 2000–January 2001). *International journal of infectious diseases*, 8(1), 27-37.
- [16] Sobarzo, A., Ochayon, D. E., Lutwama, J. J., Balinandi, S., Guttman, O., Marks, R. S., & Lobel, L. (2013). Persistent immune responses after Ebola virus infection. *New England Journal of Medicine*, 369(5), 492-493.
- [17] Heffernan, J. M., Smith, R. J., & Wahl, L. M. (2005). Perspectives on the basic reproductive ratio. *Journal of the Royal Society Interface*, 2(4), 281-293.
- [18] Leroy, E. M., Baize, S., Volchkov, V. E., Fisher-Hoch, S. P., Georges-Courbot, M. C., Lansoud-Soukate, J., & McCormick, J. B. (2000). Human asymptomatic Ebola infection and strong inflammatory response. *The Lancet*, 355(9222), 2210-2215.

[19] Muhammad Altaf, K., & Atangana, A. (2019). Dynamics of Ebola disease in the framework of different fractional derivatives. *Entropy*, 21(3), 303.

[20] Yadav, P., Jahan, S., & Nisar, K. S. (2023). Fractional order mathematical model of Ebola virus under Atangana–Baleanu–Caputo operator. *Results in Control and Optimization*, 13, 100332.

[21] Podlubny, I. (1998). Fractional differential equations: an introduction to fractional derivatives, fractional differential equations, to methods of their solution and some of their applications (Vol. 198). elsevier.

[22] Almuneef, A. A. S. (2021). Fractional derivative models for the spread of diseases.

[23] Singh, H. (2020). Analysis for fractional dynamics of Ebola virus model. *Chaos, Solitons & Fractals*, 138, 109992.

[24] Ali, A., Islam, S., Khan, M. R., Rasheed, S., Allehiany, F. M., Baili, J., ... & Ahmad, H. (2022). Dynamics of a fractional order Zika virus model with mutant. *Alexandria Engineering Journal*, 61(6), 4821-4836.

[25] Baishya, C., Achar, S. J., Veerasha, P., & Prakasha, D. G. (2021). Dynamics of a fractional epidemiological model with disease infection in both the populations. *Chaos: An Interdisciplinary Journal of Nonlinear Science*, 31(4).

[26] Berge, T., Lubuma, J. S., Moremedi, G. M., Morris, N., & Kondera-Shava, R. (2017). A simple mathematical model for Ebola in Africa. *Journal of biological dynamics*, 11(1), 42-74.

[27] Wang, X. S., & Zhong, L. (2015). Ebola outbreak in West Africa: real-time estimation and multiple-wave prediction. *arXiv preprint arXiv:1503.06908*.

[28] Webb, G. F., & Browne, C. J. (2016). A model of the Ebola epidemics in West Africa incorporating age of infection. *Journal of biological dynamics*, 10(1), 18-30.

[29] Siettos, C., Anastassopoulou, C., Russo, L., Grigoras, C., & Mylonakis, E. (2015). Modeling the 2014 ebola virus epidemic–agent-based simulations, temporal analysis and future predictions for liberia and sierra leone. *PLoS currents*, 7, ecurrents-outbreaks.

[30] Chowell, G., & Nishiura, H. (2014). Transmission dynamics and control of Ebola virus disease (EVD): a review. *BMC medicine*, 12(1), 196.

[31] Zhang, L., Addai, E., Ackora-Prah, J., Arthur, Y. D., & Asamoah, J. K. K. (2022). Fractional-Order Ebola-Malaria Coinfection Model with a Focus on Detection and Treatment Rate. *Computational and Mathematical Methods in Medicine*, 2022(1), 6502598.

[32] Gomes, M. F., y Piontti, A. P., Rossi, L., Chao, D., Longini, I., Halloran, M. E., & Vespignani, A. (2014). Assessing the international spreading risk associated with the 2014 West African Ebola outbreak. *PLoS currents*, 6, ecurrents-outbreaks.

[33] Sirirapaiwan, S., Moore, E. J., & Koonprasert, S. (2018). Generalized reproduction numbers, sensitivity analysis and critical immunity levels of an SEQIJR disease model with immunization and varying total population size. *Mathematics and computers in simulation*, 146, 70-89.

[34] Adu, I. K., Wireko, F. A., Sebil, C., & Asamoah, J. K. K. (2023). A fractal–fractional model of Ebola with reinfection. *Results in Physics*, 52, 106893.

[35] Imran, M., Khan, A., Ansari, A. R., & Shah, S. T. H. (2017). Modeling transmission dynamics of Ebola virus disease. *International Journal of Biomathematics*, 10(04), 1750057.

[36] Adu, I. K., Wireko, F. A., Nana-Kyere, S., Appiagyei, E., Osman, M. A. R. E. N., & Asamoah, J. K. K. (2024). Modelling the dynamics of Ebola disease transmission with optimal control analysis. *Modeling Earth Systems and Environment*, 10(4), 4731-4757.

[37] Yusuf, T. T., & Benyah, F. (2012). Optimal control of vaccination and treatment for an SIR epidemiological model. *World journal of modelling and simulation*, 8(3), 194-204.

[38] Lashari, A. A., & Zaman, G. (2012). Optimal control of a vector borne disease with horizontal transmission. *Nonlinear Analysis: Real World Applications*, 13(1), 203-212.

[39] Seck, R., Ngom, D., Ivorra, B. P. P., & Ramos Del Olmo, Á. M. (2021). An optimal control model to design strategies for reducing the spread of the Ebola virus disease.

[40] Raissi, M., Perdikaris, P., & Karniadakis, G. E. (2019). Physics-informed neural networks: A deep learning framework for solving forward and inverse problems involving nonlinear partial differential equations. *Journal of Computational physics*, 378, 686-707.

[41] Willard, J., Jia, X., Xu, S., Steinbach, M., & Kumar, V. (2022). Integrating scientific knowledge with machine learning for engineering and environmental systems. *ACM Computing Surveys*, 55(4), 1-37.

[42] Tang, Y., Kurths, J., Lin, W., Ott, E., & Kocarev, L. (2020). Introduction to focus issue: When machine learning meets complex systems: Networks, chaos, and nonlinear dynamics. *Chaos: An Interdisciplinary Journal of Nonlinear Science*, 30(6).

[43] Sarumi, O. A. (2020, December). Machine learning-based big data analytics framework for ebola outbreak surveillance. In *International conference on intelligent systems design and applications* (pp. 580-589). Cham: Springer International Publishing.

[44] Igoe, M., Casagrandi, R., Gatto, M., Hoover, C. M., Mari, L., Ngonghala, C. N., ... & de Leo, G. (2023). Reframing optimal control problems for infectious disease management in low-income countries. *Bulletin of mathematical biology*, 85(4), 31.

[45] Kochańczyk, M., & Lipniacki, T. (2021). Pareto-based evaluation of national responses to COVID-19 pandemic shows that saving lives and protecting economy are non-trade-off objectives. *Scientific reports*, 11(1), 2425.

[46] Broekaert, J. B., La Torre, D., & Hafiz, F. (2024). Competing control scenarios in probabilistic SIR epidemics on social-contact networks. *Annals of Operations Research*, 336(3), 2037-2060.

[47] Li, Y., Chen, Y., & Podlubny, I. (2010). Stability of fractional-order nonlinear dynamic systems: Lyapunov direct method and generalized Mittag–Leffler stability. *Computers & Mathematics with Applications*, 59(5), 1810-1821.

[48] Xia, Z. Q., Wang, S. F., Li, S. L., Huang, L. Y., Zhang, W. Y., Sun, G. Q., ... & Jin, Z. (2015). Modeling the transmission dynamics of Ebola virus disease in Liberia. *Scientific reports*, 5(1), 13857.

[49] Goeijenbier, M., Van Kampen, J. J., Reusken, C. B., Koopmans, M. P., & Van Gorp, E. C. (2014). Ebola virus disease: a review on epidemiology, symptoms, treatment and pathogenesis. *Neth J Med*, 72(9), 442-8.

[50] Chowell, G., & Nishiura, H. (2014). Transmission dynamics and control of Ebola virus disease (EVD): a review. *BMC medicine*, 12(1), 196.

[51] Lau, M. S., Dalziel, B. D., Funk, S., McClelland, A., Tiffany, A., Riley, S., ... & Grenfell, B. T. (2017). Spatial and temporal dynamics of superspreading events in the 2014–2015 West Africa Ebola epidemic. *Proceedings of the National Academy of Sciences*, 114(9), 2337-2342.

[52] Berge, T., Lubuma, J. S., Moremedi, G. M., Morris, N., & Kondera-Shava, R. (2017). A simple mathematical model for Ebola in Africa. *Journal of biological dynamics*, 11(1), 42-74.

[53] Van den Driessche, P., & Watmough, J. (2002). Reproduction numbers and sub-threshold endemic equilibria for compartmental models of disease transmission. *Mathematical biosciences*, 180(1-2), 29-48.

- [54] Pillai, S. U., Suel, T., & Cha, S. (2005). The Perron-Frobenius theorem: some of its applications. *IEEE Signal Processing Magazine*, 22(2), 62-75.
- [55] Kamocki, R. (2014). On the existence of optimal solutions to fractional optimal control problems. *Applied Mathematics and Computation*, 235, 94-104.
- [56] Agrawal, O. P., Defterli, O., & Baleanu, D. (2010). Fractional optimal control problems with several state and control variables. *Journal of Vibration and Control*, 16(13), 1967-1976.